



PERGAMON

Deep-Sea Research II 49 (2002) 3889–3915

DEEP-SEA RESEARCH
PART II

www.elsevier.com/locate/dsr2

Zooplankton distribution and behaviour in the Southern Ocean from surveys with a towed Optical Plankton Counter

R.T. Pollard^{a,*}, U. Bathmann^b, C. Dubischar^b, J.F. Read^a, M. Lucas^a

^aSouthampton Oceanography Centre, Waterfront Campus, European Way, Southampton SO14 3ZH, UK

^bAlfred Wegener Institut für Polar- und Meeresforschung, D-27515, Bremerhaven, Germany

Received 17 December 1998; received in revised form 25 April 2001; accepted 15 May 2001

Abstract

Spatial distributions of zooplankton with lengths between about 500 μm and 8 mm are described from surveys in the vicinity of the Antarctic Polar Front in austral summer 1995/6 using an Optical Plankton Counter mounted on a towed profiling SeaSoar. The distributions, split into several logarithmically spaced size classes, are compared and related to the physical environment south of the Polar Front in the Antarctic Zone and within the Polar Frontal Zone. They also are compared with phytoplankton distributions determined from surface chlorophyll data. Both phytoplankton and zooplankton carbon densities are low in the Antarctic Zone ($2\text{--}3\text{ g C m}^{-2}$), but rise to larger values in the Polar Frontal Zone ($5\text{--}7\text{ g C m}^{-2}$ for zooplankton and a maximum of 6 g C m^{-2} at fronts for phytoplankton). Calibration of OPC derived zooplankton biovolume to carbon was achieved by comparison with dry weights from multinet samples deployed in conjunction with CTD casts. The net data showed that over 98% of zooplankton counts were copepods. Diel behaviour also was examined. Only larger copepods (over 2 mm long) displayed significant diel migration, and then only 10–20% of the standing stock; the majority remained deeper than about 100 m and their distribution patterns suggest that they may be retained aside from the main frontal jets by ageostrophic circulations associated with the front. Copepods shorter than 2 mm rose from depth over the month-long survey to become concentrated in the surface layer (the top 70–100 m). The largest copepods that could be resolved, with lengths of about 4–8 mm (possibly *Rhincalanus gigas*), displayed unexpected behaviour in tending to migrate to the top 0–10 m by day, descending to 40–50 m each night. © 2002 NERC. Published by Elsevier Science Ltd. All rights reserved.

1. Introduction

Investigation of the spatial distribution of pelagic organisms is usually hampered by biological patchiness and very time-consuming sampling procedures. While satellite-based observations of the pigment distribution in surface waters has

greatly improved our knowledge of the spatial distribution of phytoplankton, zooplankton patterns are not detectable with this method. But recently, our ability to conduct mesoscale surveys of zooplankton distribution has been enhanced considerably by the development of the Optical Plankton Counter (OPC) (Herman, 1988, 1992; Herman et al., 1991). The OPC can be lowered on a CTD or net (which is essential for biological calibration), but is more powerfully used by mounting it on a towed vehicle such as Batfish

*Corresponding author. Tel.: +44-23-8059-6433; fax: +44-23-8059-6015.

E-mail address: rtp@soc.soton.ac.uk (R.T. Pollard).

(Herman et al., 1991) or SeaSoar (Huntley et al., 1995). Huntley et al. (1995) reported the first use of the OPC on a SeaSoar. Here we report what we believe to be the first mesoscale survey in the Southern Ocean with an OPC mounted on a SeaSoar (Pollard, 1986), although transects across the Southern Ocean using an OPC mounted in-board on a ship have been reported (Gallienne et al., 1996).

Although the Southern Ocean is considered to be an HNLC (high nutrient, low chlorophyll) region, the Polar Frontal Zone is one with relatively high biological productivity, where, for example, chlorophyll values of up to $4 \mu\text{g l}^{-1}$ were found during austral spring 1992 (Bathmann et al., 1997). Zooplankton grazing by the dominant larger copepod species was very low and accounted for <1% of the daily primary production in this period (Dubischar and Bathmann, 1997). Phytoplankton blooms with different dominant species occurred relatively close to each other (Bathmann et al., 1997), indicating high spatial heterogeneity. The SO-JGOFS *Polarstern* cruise during austral summer 1995/6 was carried out to investigate this frontal system on smaller scales, linking physical and biological parameters. This paper deals mainly with the distribution of zooplankton organisms in relation to hydrography. We try to answer the following questions:

- is the distribution of the different zooplankton organisms caused by the hydrographic situation in the area surveyed?
- what is the role of the observed zooplankton distribution on smaller scales in the ecosystem?

We begin with an overview of the SeaSoar surveys in the vicinity of the Antarctic Polar Front to set the physical context, then introduce the OPC processing, first using very large bin sizes (90 m^3) to examine the OPC's ability to sample larger zooplankton (up to about 20 mm in length). More detail on species composition, spatial distribution and diel behaviour of the smaller zooplankton (up to 8 mm length) is then described using smaller bins and the vertical and temporal structure of zooplankton distribution in three main physical zones is derived. Using data from these zones, it is possible to calibrate the OPC data in terms of

zooplankton carbon. Finally, the inter-relations between the various sizes of zooplankton and phytoplankton distributions are discussed relative to the physical environment.

2. SeaSoar surveys and the hydrographic situation

The data presented here were collected on cruise AntXIII/2 of the German research ship *Polarstern* between 6 December 1995 (day 340) and 5 January 1996 (day 370). Data were collected on four surveys (Fig. 1 and Table 1). Surveys 2 and 3 were long transects extending from the Subtropical Front at 39°S to the Antarctic Polar Front (APF) at 50°S and from the APF to the northernmost extent of sea-ice cover at 57°S . The long transects are discussed in more detail elsewhere (Read et al., 2002).

Run 6 (Fig. 1b), the Coarse Scale Survey (CSS), repeated part of Survey 3 from 54°S to the APF (Leg 6.1) followed by 6 legs (6.2–6.7) across the APF spaced 75 km apart and ranging from 200–250 km long. Survey 8 (Fig. 1c), the Fine Scale Survey (FSS), consisted of 11 legs 13 km apart and 120 km long covering the northeast corner of Survey 6. Leg 8.1 duplicated part of Leg 6.7 and Leg 8.7 likewise re-occupied part of Leg 6.6. The SeaSoar data are fully reported by Griffiths et al. (1996). Several CTD casts taken at the beginning and end of SeaSoar runs (CTDs 6, 7, 9) are marked on Fig. 1, as are casts taken in the CSS area between or after the surveys (CTDs 15–18) and CTD 22 on a line of CTDs (CTDs 20–29) repeating Leg 8.7 of the FSS.

Potential temperature (from a Neil Brown Mark 3 CTD) extracted at the depth of the temperature minimum (120–220 m) is superimposed on Figs 1b and c as a guide to the locations of major fronts. The strongest horizontal temperature gradients are from 1.4°C down to 0.4°C , and we shall show that the 1°C temperature minimum marks a significant boundary between low zooplankton and phytoplankton biomass on the colder side and significantly higher biomass on the warmer side. Acoustic Doppler Current Profiler (ADCP) data (Naveira Garabato et al., 2001; Read et al., 2002; Strass et al., 2002) show a current jet running

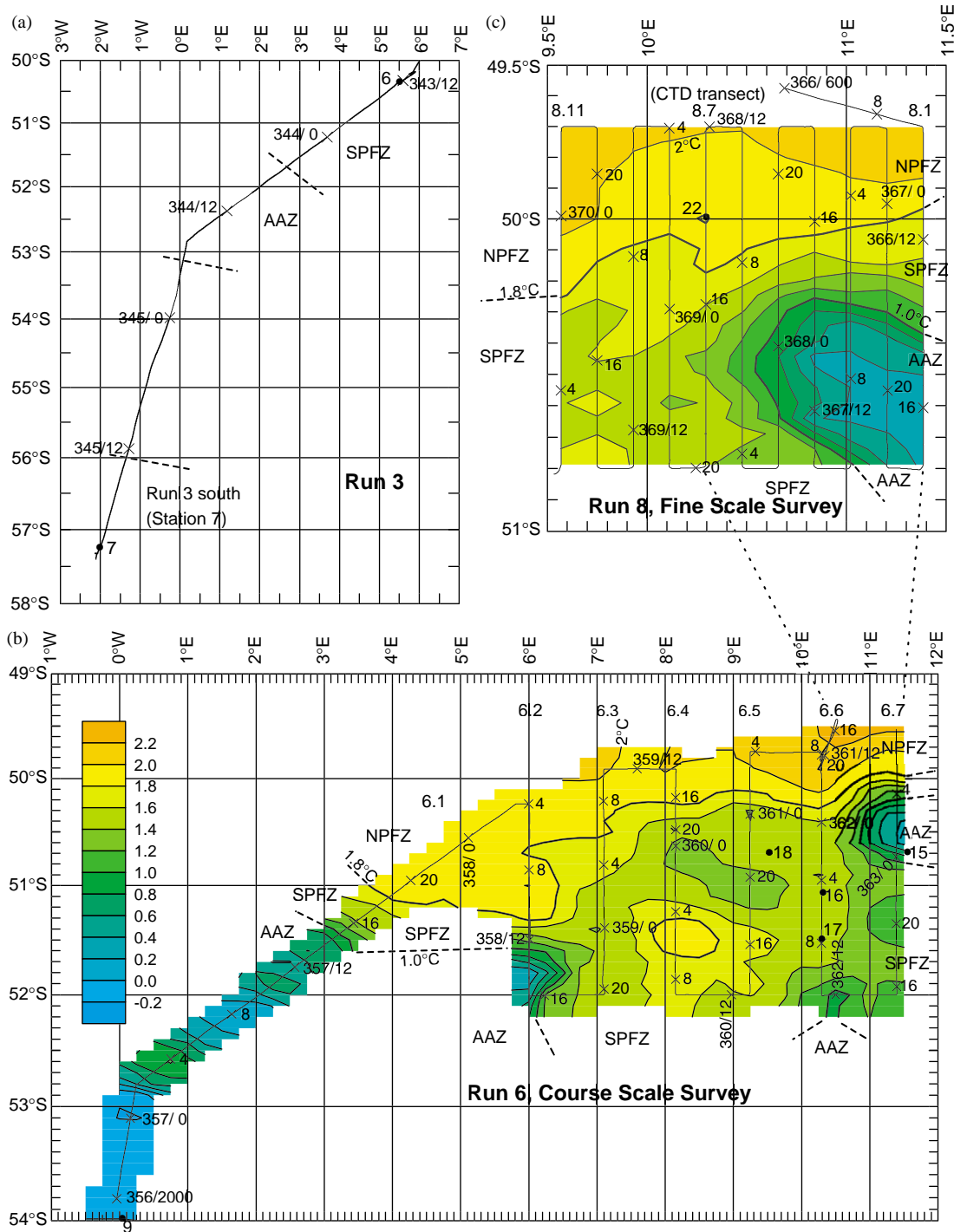


Fig. 1. Track plots of (a) Run 3, (b) Run 6, the Coarse Scale Survey, (c) Run 8, the Fine Scale Survey. Times (GMT) are marked by crosses and day of year (in 1995, so 366 is 1 January 1996) is annotated at 0 and 12 h daily. Contours of potential temperature (0.2°C intervals) at the temperature minimum are superimposed on (b) and (c) and the 1.0 and 1.8°C isotherms are used (see text) to delineate three inter-frontal zones, the Antarctic Zone (AAZ), Southern Polar Frontal Zone (SPFZ) and Northern Polar Frontal Zone (NPFZ). CTDs (bold dots) used for OPC calibrations are numbered.

Table 1
SeaSoar/OPC surveys

| | Duration (days, h) | Distance run (km) | OPC counts | Latitude bounds | | Day of year in 1995 |
|----------|--------------------|-------------------|------------|-----------------|----------|---------------------|
| | | | | Northern | Southern | |
| Survey 2 | 2 d 17.5 h | 1091 | 2,577,212 | 41°47'S | 50°13'S | 340–343 |
| Survey 3 | 2 d 6.8 h | 990 | 2,945,368 | 50°21'S | 57°20'S | 343–345 |
| Survey 6 | 6 d 2.4 h | 2529 | 9,823,772 | 49°28'S | 54°01'S | 357–363 |
| Survey 8 | 3 d 21.0 h | 1471 | 6,908,434 | 49°41'S | 50°48'S | 366–370 |
| TOTAL | 14 d 23.7 h | 6081 | 22,234,786 | | | |

eastwards along this front at speeds of up to 30 cm s^{-1} . The front extends eastwards along 51.5°S as far as 6.5°E before turning sharply southwards out of the Coarse Scale Survey area. It reappears at 50.5°S as an eddy or meander at the easternmost edge of both the Coarse and Fine Scale Surveys, again with clear cyclonic (clockwise) currents (Vélez et al., 2002).

Read et al. (2002) concludes that this front is the surface expression of the APF, distinguishing it from the subsurface expression of the APF further north. The distinction is necessary because the APF is most commonly determined by the location of the subsurface 2°C temperature minimum (Belkin and Gordon, 1996), where we have used 1°C . Pollard et al. (2002) re-examine the zonation of the Southern Ocean and conclude that the current jets of the ACC, which frequently split and merge (Pollard and Read, 2001), cannot reliably be mapped onto scalar features (such as the 2°C temperature minimum). Scalar features can be circumpolar. The current jets of the ACC such as the APF are not circumpolar, only the total ACC transport. Read et al. (2002) and Strass et al. (2002) also note the stronger currents (up to 50 cm s^{-1}) at the subsurface expression of the APF and the downturning of the temperature minimum to the north where that front is crossed at 49°S , 7°E . Examining Figs 1b and c, we find that neither the CSS nor FSS extended fully across the APF to its north side, although the 2°C temperature minimum does appear at the northern end of most legs of each survey.

For the purposes of this paper, however, we note that there is a somewhat enhanced horizontal temperature gradient between the 1.6°C and 1.8°C

temperature contours in Fig. 1b, and ADCP data (Allen et al., 1996) show enhanced eastward currents on Legs 6.3–6.5 between 50 and 50.5°S , which continue eastwards at around 50°N on Legs 6.6–6.7. We shall therefore take the 1.8°C temperature minimum as a possible physical boundary, so that we may compare zooplankton biomass north of the 1.8°C isotherm, between the 1.8°C and 1.0°C isotherms, and south of the 1.0°C isotherm. We shall refer to the coldest zone, south of the 1.0°C isotherm, as the Antarctic Zone (AAZ) (Belkin and Gordon, 1996). The two warmer zones both lie between the surface and subsurface expressions of the APF, usually referred to in biological literature as the Polar Frontal Zone (PFZ). To distinguish the two zones, we shall refer to them here as the Northern Polar Frontal Zone (NPFZ) and Southern Polar Frontal Zone (SPFZ).

3. Methods—OPC data collection and processing

AntXIII/2 was the first cruise in Antarctic waters on which a Focal Technologies OPC was fitted beneath the SeaSoar (Pollard, 1986). SeaSoar was towed behind the *Polarstern* at 4 m s^{-1} , profiling between the surface 350 – 375 m and back approximately every 15 – 20 min . The OPC was additional to the normal SeaSoar payload of a Neil Brown Mark 3 CTD, a Chelsea Instruments Fluorometer and a PAR upward looking light sensor. The OPC installation worked extremely well and over 22 million OPC counts were recorded during 15 days of surveying (Table 1). This paper provides an overview of this extensive

OPC data set, examining its distribution by size class, depth, geographical position, and time, all in relation to the physical water properties recorded by the CTD.

The OPC data were logged by PC (Focal Technologies manual) to a disc drive connected to a Sun Workstation. The OPC records particles with equivalent spherical diameters (ESDs) between 0.25 and 12 mm (Herman, 1992). Up to 100–200 counts per second can be recorded before coincidence counts become a problem. The ship's master clock was added to the data stream every second to ensure that the time base of the CTD and OPC were exactly synchronised. The individual counts were not time-stamped by the PC, but we added a time-stamp to aid data processing by arbitrarily dividing each second into as many even intervals as there were counts. Further details are given in Pollard et al. (1996).

In order to obtain zooplankton calibration data, a Multinet with 100 μm mesh-size capable of collecting 5 samples was deployed at most CTD stations (Dubischar et al., 1997). Depth intervals for sampling were generally 0–25, 25–50, 50–100, 100–300, and 300–500 m. An OPC similar to that mounted on SeaSoar was attached to the Multinet, the primary difference being that the net-mounted OPC had an aperture of 3 cm \times 22 cm, whereas that on the SeaSoar was only 2 cm \times 5 cm to avoid coincidence counts at the 4 m s^{-1} towing speed. Clearly it is not possible to carry out a direct comparison of Multinet data with the SeaSoar-mounted OPC, because they could not be used simultaneously, nor at exactly the same location. Instead, we shall compare OPC data averaged in the three frontal zones (AAZ, SPFZ and NPFZ) with Multinet data from CTDs in those zones in order to arrive at a calibration of the OPC in terms of zooplankton carbon densities. This comparison must be deferred until the spatial structure of the data has been described.

However, this paper is mostly concerned with distribution patterns, i.e. the relative contributions of different size classes, spatial, temporal, and depth variations, for which absolute calibration is not essential. Through most of the paper, therefore, OPC data will be presented in terms of biovolume in units of mm^3/m^3 (or parts per

billion), having converted the raw counts to spherical volumes using the default lookup table developed by Herman (1992) and given in the instrument handbook. We have calculated sample volumes by using the known OPC aperture and assuming that the speed of SeaSoar through the water is the same as the ship speed. In fact SeaSoar travels faster than the ship as it profiles from the surface to 350 m, but the error is small except when SeaSoar descends rapidly, and this is countered in our analysis by our temporal averaging which includes both down and up casts.

The net data revealed that the vast majority of zooplankton (over 98%) counted were copepods or copepodites, with near-negligible contributions from chaetognaths, polychaetes, euphausiid larvae, salps, and detritus such as faecal pellets. The net data will thus be used to discuss which species and stages of copepods are prevalent in each OPC size class, bearing in mind that ESD and animal length are related by ($\text{ESD}^2 = \text{length} \times \text{width}$) (Herman, 1992). Thus, if the length of each copepod is four times the width, then its length is exactly twice its ESD. We shall use this conversion as a guide although the length is typically more like three times the width for the copepods measured.

4. Results—distribution by size class

As a first step to check whether the OPC is indeed able to obtain representative sample of copepods with ESDs between 250 μm and 12 mm (i.e. lengths between about 0.5 and 24 mm), we have binned all 22 million counts (Table 1) regardless of depth into 6-hourly sums in 6 logarithmically scaled size classes, each double the previous: 250–500 μm , 0.5–1.0, 1–2, 2–4, 4–8 and >8 mm (Table 2 and Fig. 2). Given that the aperture of the OPC through which particles must pass is 2 cm \times 5 cm, or 0.001 m^2 , and that the mean ship speed is just over 4 m s^{-1} , in 6 h the ship has travelled 90 km and the OPC has sampled about 90 m^3 of water. We have used this large sample volume to attempt to obtain reliable statistics for the larger size classes.

Table 2
OPC size class distribution averaged over all surveys

| Size class ESD | Average no. in sample ^a | Std. deviation of no. in sample | Empty samples ^b | Average biovol (mm ³ m ⁻³) | Relative biovol |
|----------------|------------------------------------|---------------------------------|----------------------------|---|-----------------|
| 250–500µm | 196,338 | 72105 | 0 | 63.9 | 17% |
| 500–1000µm | 75,481 | 28462 | 0 | 132.7 | 35% |
| 1–2 mm | 9602 | 4057 | 0 | 125.1 | 33% |
| 2–4 mm | 476 | 238 | 0 | 41.1 | 11% |
| 4–8 mm | 19 | 17 | 0 | 15.7 | 4% |
| over 8 mm | 7 | 15 | 13 | 136.1 | omitted 100% |

^a Sample size was 6 h sum of all OPC counts at all sampled depths. Mean volume in sample was 90 m³.

^b There were 58 6-h samples altogether.

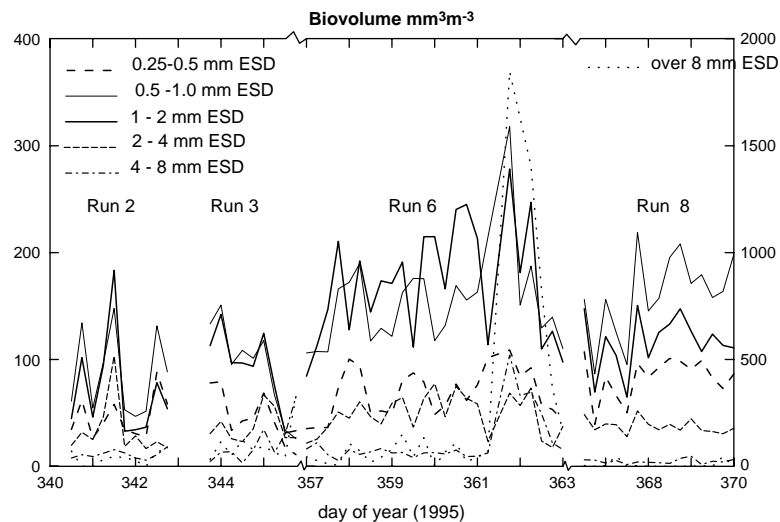


Fig. 2. Biovolume (in mm³ m⁻³, or parts per billion) plotted against time for 6 h (about 90 m³) bins (spanning all depths from 0–360 m) and 6 size classes. The equivalent spherical diameter (ESD) of the smallest size class spans 250–500 µm and doubles for each successive size class up to 4–8 mm ESD. The largest size class contains data from 8–12 mm ESD and is plotted on a considerably compressed (factor of 5) vertical scale (shown on the right-hand axis).

For the largest size class, particles with ESD > 8 mm, it is clear from Table 2 that even 90 m³ is not a large enough sample. Out of 58 samples, 13 had no particles in them, with an average of 7 individuals per sample and a standard deviation of 15 individuals per sample. Thus the towed OPC cannot well resolve the spatial distribution of large particles in our survey area. The next smaller size class 4–8 mm ESD is just resolved, averaging 19 counts per sample with a standard deviation of 17 counts per sample. There are however two anomalies.

At the southernmost limit of SeaSoar surveying (day 345.75, Fig. 2) at 57°S (determined by sea ice), these two size classes both have unusually large biovolume. Classes with ESD < 2 mm have unusually low biovolume. The second anomalous period is from day 361.75 to 363, which covers the last two legs of the Coarse Scale Survey 6 (Fig. 1b). Biovolumes in all size classes reach maxima, with the > 8 mm class registering counts of 66, 68 and 65 individuals in 3 consecutive 6 h periods, with biovolumes of 1400–1800 mm³ m⁻³, 6–10 times larger than in any other size class. The most likely

explanation for both anomalous periods is that swarms of euphausiids were encountered. Small numbers (typically $5\text{--}20\text{ ind m}^{-3}$ in the 25–50 m net) of euphausiid larvae were regularly found in net samples. The anomalies provide evidence that the OPC can and does sample animals as large as 12 mm ESD when they are present, possibly because its speed through the water minimises their opportunity for avoidance manoeuvres.

The size class 2–4 mm ESD has an average of 476 counts per sample, so would be well-resolved with smaller bin sizes. If the sample period is reduced to 1 h, one would expect 80 counts per sample, so some vertical resolution is also possible. In the next section we shall use 20 m bins in the vertical and examine the distributions of the four smallest size classes, up to 4 mm ESD. If we exclude the > 8 mm size class from total biovolume calculations, then the 2–4 mm class contributes on average 11% of the biovolume. Its largest value occurs at day 341.5 (Fig. 2) in an eddy south of the Subtropical Front, which is discussed further by Read et al. (2002).

The size classes 0.5–1 mm and 1–2 mm contain 35% and 33% of the biovolume averaged over all surveys, or 2/3 of the biovolume in the range sampled by the OPC. The smallest size class sampled, 250–500 μm , contributes only 17% of the biovolume and may be undersampled by the OPC because of its cutoff near 250 μm (Herman, 1992). Note also that the numbers of smaller particles are not so large as to saturate the OPC's counting ability. If particles pass through the OPC's aperture at rates $> 100\text{--}200\text{ s}^{-1}$ (Herman, 1992), their shadows can merge, leading to counts in a larger size class. From Table 2 we can infer that the average count rate is 13 s^{-1} , well below the limit. However, in the surface layers, counts were typically 50 s^{-1} , so that, without the restriction to the aperture for the towed OPC, counts would have saturated.

In summary, the overall shape of Table 2 is encouraging, as a fairly accurate representation of zooplankton distribution over the whole stated range of the OPC, although we have no way of quantifying possible avoidance of either the towed OPC or the Multinet. While the total number of animals in a sample is dominated by the smallest size class, the biovolume distribution over the six

logarithmic size classes is relatively flat, as theory says it should be in the global mean (Sheldon et al., 1972). Obviously, such a relationship does not hold in a local area sampled over a limited period, but the reduction in percentage contribution of the size classes with ESDs $> 2\text{ mm}$ is probably real, as anomalous swarms of larger animals were observed on occasion. The primary limitation on the OPC's ability is that it cannot sample large enough volumes of water to provide full mesoscale resolution of the larger size classes unless they are populated unusually densely.

One final comment is that OPC data are frequently quoted in terms of ind m^{-3} . It is clear from Table 2 that any statement based on counts is hugely biased to the smallest sizes of zooplankton. For that reason, we consider it greatly preferable to use biovolume. Mention of ind m^{-3} (individuals per m^3) will be restricted to (a) comparisons with net data, and (b) ensuring that sample volumes contain enough individuals for reliable statistics.

5. Temporal and spatial distributions by size class and species composition

We next regridded the OPC data using the same size classes but with finer bins: 1 h long to resolve diel behaviour; 20 m in the vertical to examine depth dependence. The same gridding has been applied to potential temperature (Fig. 3) and contours for the four size classes 0.25–0.5, 0.5–1, 1–2 and 2–4-mm ESD are shown against time and depth in Figs. 4–7, using the same colour scales for all four figures. The data set is an intricate mix of time and space, and the reader must be aware always that apparent temporal changes in Figs. 4–7 may in fact be spatial changes as the surveys crossed and recrossed frontal boundaries. Maps of the FSS (Fig. 8) and CSS (Fig. 9) help to clarify this. Frequent cross-reference between the times on Figs. 3–7 and their positions on Fig. 1 is recommended. Note for example that part (b) of each figure from day 357 forward is the exact reverse in space of part (a) from day 345 backwards, i.e. there is a 12–14-day time gap. Potential temperature isotherms of 1.0°C and 1.8°C have been added to the figures to aid the discrimination

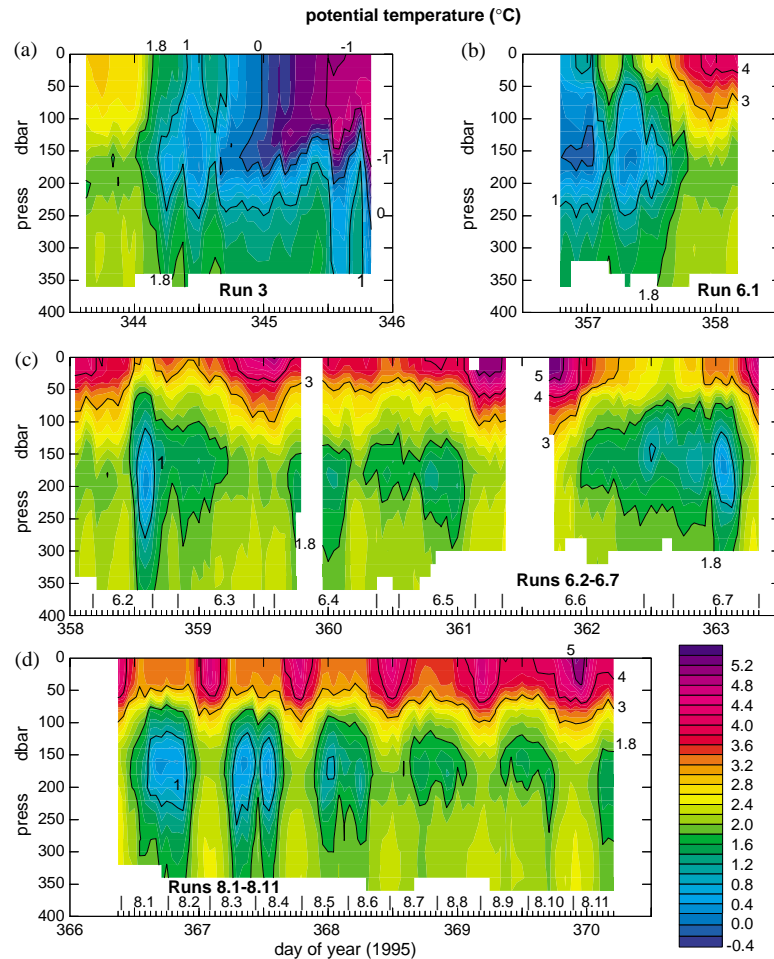


Fig. 3. Potential temperature contoured against time and depth for (a) Run 3, (b) the first leg of the Coarse Scale Survey, Run 6.1, (c) the remainder of the CSS, Runs 6.2–6.7 (gaps mark periods when the SeaSoar had to be recovered for cable repairs) and (d) the Fine Scale Survey, Runs 8.1–8.11. The start and end of each run is marked. Hourly tick marks show the centres of the hourly bins. Temperature contours are shown at -1 , 0 , 1 , 1.8 , 3 , 4 and 5°C .

of time and space. Approximate start and end of each leg have also been marked. From Fig. 3d, for example, the temporal locations of the eleven legs of the FSS (Fig. 1c) are easily inferred from the cold subsurface temperature minima (from 150–200 m) at the southern ends of legs 8.1–8.2, 8.3–8.4 and so forth.

5.1. 0.25–0.5 mm ESD

The dominant individual component of the smallest size class (0.25–0.5 mm, Fig. 4) is prob-

ably *Oithona* spp (Table 3), a cyclopid copepod whose adult size is just smaller than 0.5 mm ESD. A maximum of 1000 ind m^{-3} of adult females were counted in the 25–50 m net at one station, which equates to a biovolume of about $60 \text{ mm}^3 \text{ m}^{-3}$. Other major contributors in the Multinet samples are adult females of *Microcalanus pygmaeus* and copepodites of slightly larger animals such as *Ctenocalanus* and *Clausocalanus* (Table 3). More detail is given in Dubischar et al. (2002).

This size class is largely confined to the weakly stratified surface layer, where its biovolume can be

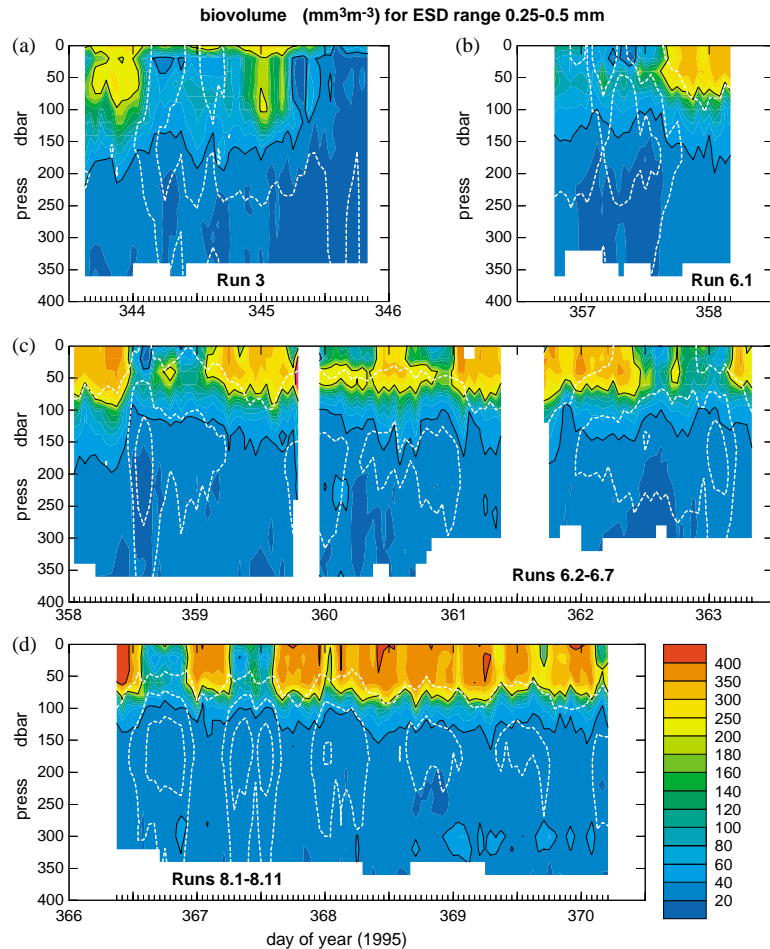


Fig. 4. Zooplankton biovolume for the ESD size range 0.25–0.5 mm contoured as for Fig. 3. In addition to colour shading, contour lines are shown for biovolumes of 40, 200 and 400 mm^3m^{-3} . Potential temperature contours (Fig. 3) for 1.0°C and 1.8°C are superimposed as dotted white lines.

as large as 400 mm^3m^{-3} (Fig. 4), or over 13000 ind m^{-3} (deduced from Table 1). During Run 3, the pycnocline was as deep as 150 m or even 200 m (Read et al., 2002) and biovolume in this size class extended to that depth (Fig. 4a). By Run 8 (Fig. 4d) the pycnocline had risen to about 80 m, and biovolume was evenly distributed above that depth. Areas of low biovolume in the surface layer (e.g., Fig. 4c around day 358.6; Fig. 4d, days 366.7 and 367.5) are directly correlated with the frontal structure, being confined to areas where the temperature minimum is < 1.8°C (Fig. 8a) or even 1.0°C in the southeast corner of the FSS. Where

the surface layer values are low, however, they tend to be unevenly distributed with depth, having a maximum subsurface towards the base of the weakly stratified layer and often a maximum also in the top 10 m.

Copepods in the Southern Ocean at 50°S in this size class show diurnal vertical migration in summer of a few tens of meters only (Metz, 1996), with a migration speed of a few cm per minute. Physical (wind-driven) mixing is therefore probably primarily responsible for the even vertical distribution down to the pycnocline (say 100 m) in most areas. Note however that these

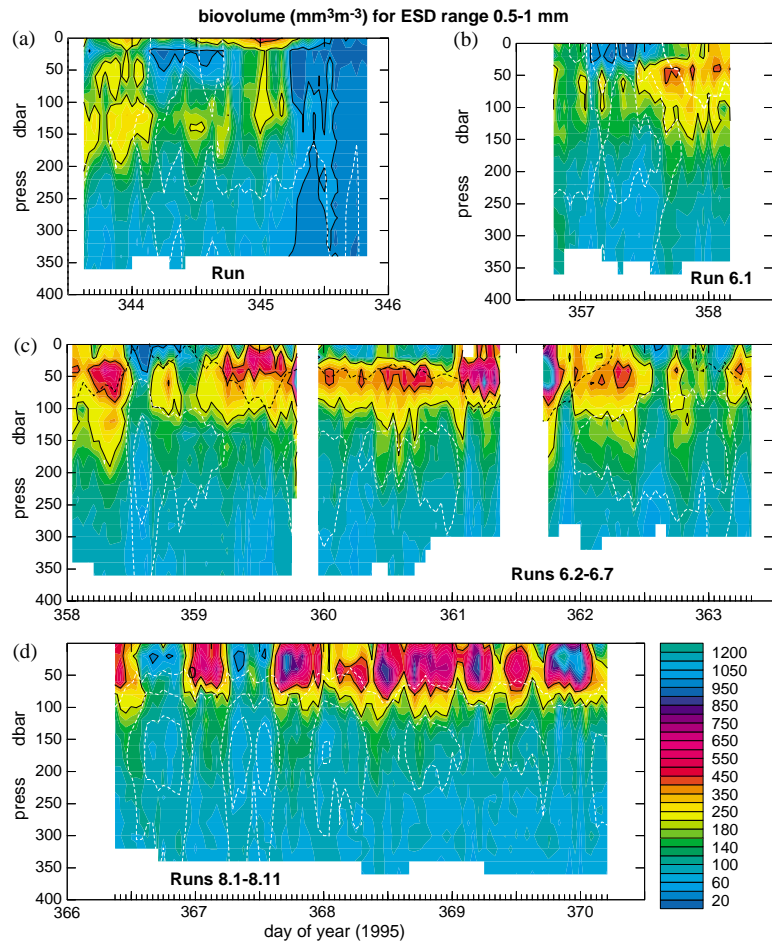


Fig. 5. As for Fig. 4, but for the ESD size range 0.5–1 mm.

small copepods are still present in significant numbers below the surface layer. Even at 300 m (e.g., Fig. 4d, day 369) biovolume can exceed $40 \text{ mm}^3 \text{ m}^{-3}$ requiring counts of over 600 ind m^{-3} .

5.2. 0.5–1 mm ESD

Numerous species of copepods contribute to this size class (Fig. 5), including adult females of *Ctenocalanus* and *Clausocalanus*, possibly large *Oithona*, and copepodites of larger species such as *Calanoides acutus*, *Calanus propinquus*, *C. similis*, *Metridia lucens*, and *M. gerlachei* (Table 3). This size class again tends to be confined to the

surface layer, particularly by the time of the FSS (Fig. 5d) but less so than the 0.25–0.5 mm size class. In particular, there is evidence for a deep subsurface maximum, centred around 100–200 m on day 344 (Fig. 5a), rising through 100 m (at the same spatial position) on day 358 (Fig. 5b) and merging into the surface layer maximum in the FSS (Fig. 5d). We speculate that this could be a late breeder such as *M. lucens* rising towards the surface to breed. Certainly, Dubischar et al. (2002) counted significant numbers of adult female *M. lucens* with eggs in the net samples at most stations in the CTD transect after the FSS (Fig. 1c).

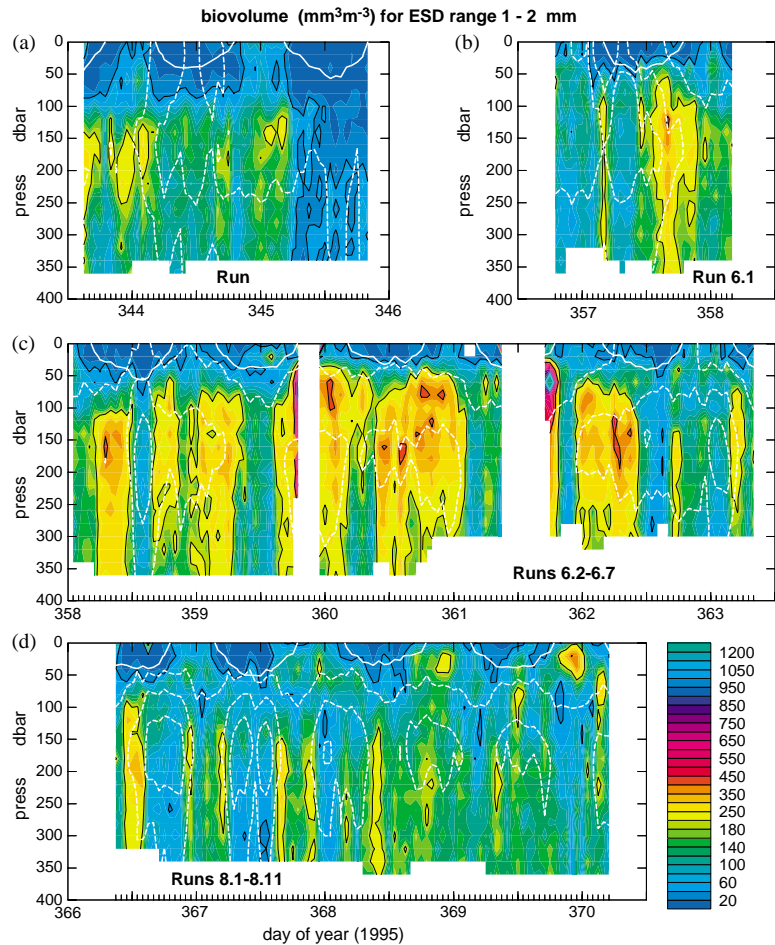


Fig. 6. As for Fig. 4 but for the ESD size range 1–2 mm. To indicate day and night, the 5 Wm^{-2} isolume from the PAR sensor on SeaSoar is superimposed as a solid white line.

Spatially (Fig. 8b), the distribution of this size class is very similar to that of the 0.25–0.5 mm size class. Unlike the smaller size class, though, the 0.5–1 mm class is not evenly distributed with depth through the surface layer. In Fig. 10 are presented profiles of several size classes averaged by day and by night over the whole of each of the Coarse and Fine Scale Surveys. The data were first gridded to 2 m vertical resolution (compared to the 20 m in Fig. 5) in the top 120 m then temporally (horizontally) averaged. In Run 6 (Fig. 10a), there is a single subsurface peak in biovolume centred at 40–50 m, with values two or three times higher at that depth than at the minimum around 10 m deep.

Thus these animals tend to avoid the very surface layer. In Run 8 (Fig. 10b), in addition to the peak at 40–50 m, a shallower peak has appeared between 20 and 30 m, but again values fall off in the top 10–20 m. It is likely that the two peaks in Run 8 are caused by different species, but the depth resolution of the Multinet casts is unfortunately insufficient to resolve the two peaks.

While there are large differences between the day- and night-time profiles in Fig. 10 for the 0.5–1 mm size class, we do *not* ascribe these to diel migration. In Run 6 the night-time values for this size class are *smaller* than the day-time values, and in both surveys it is clear (by comparing the areas

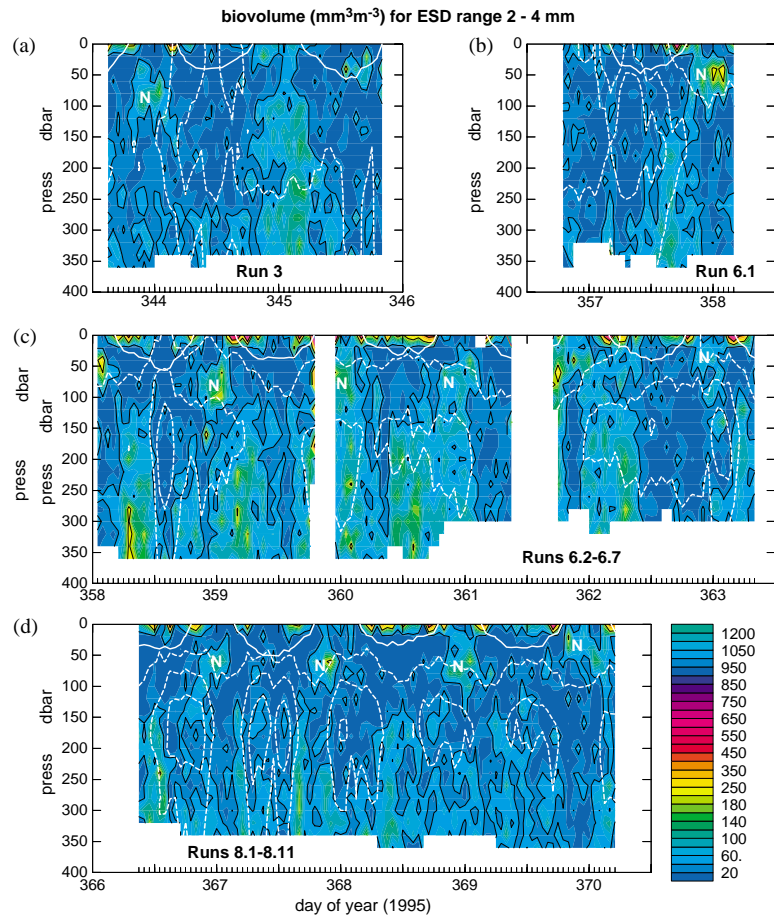


Fig. 7. As for Fig. 6 but for the ESD size range 2–4 mm. Nocturnal concentrations in the surface layer are marked N.

under the curves) that there are considerable differences between the vertically integrated day- and night-time biovolumes. The differences must thus be spatial, not temporal, and Fig. 8 provides the evidence. Fig. 8c is a convenient way of distinguishing day and night on a map. Fig. 8e is mapped at the depth of the 20–30 m depth peak for the 0.5–1 mm size class in the CSS (Fig. 10b) and shows that the three spatial peaks of biomass (at the northwest corner of the survey area, at the northern edge of the survey around 10.7°E and at the southern edge of the survey around 10.3°E) all happened to be surveyed at night. This explains the large night-time peaks in Fig. 10b. We conclude that this size class exhibits little or no diel vertical migration.

5.3. 1–2 mm ESD

A very different picture is presented by this size class (Fig. 6), representing copepods with lengths of order 2–4 mm. Adults of *Metridia lucens*, *M. gerlachei*, *Pleuromamma robusta*, and *Calanus simillimus* fall in this class, as do larger stages of *Calanoides acutus*, *Calanus simillimus* and *Rhinca lanus gigas* (Table 3). Larger stages of *Calanus propinquus* also fall in this size class, but this southern species was found only at the southern ends of Runs 3 and 6, well south of the Polar Front. In contrast to the smaller size classes, most of the biovolume in this class remains below the surface layer (the top 50–100 m) at all times, as is particularly apparent in the CSS (Fig. 6c), which is

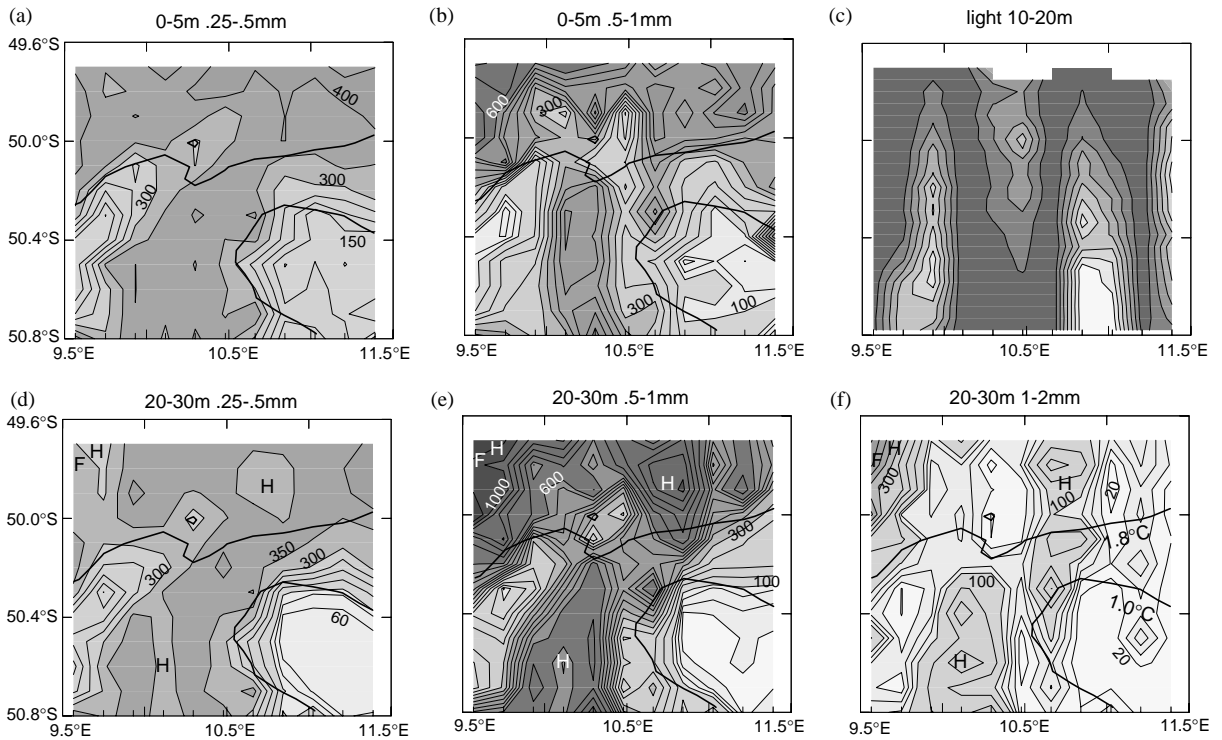


Fig. 8. Fine Scale Survey area maps of (a) 0.25–0.5 and (b) 0.5–1 mm ESD in the depth range 0–5 m; (c) isolines at 20 m depth; (d) 0.25–0.5, (e) 0.5–1 and (f) 1–2 mm ESD in the depth range 20–30 m. Isolines on (c) are at 5 Wm^{-2} intervals. Biovolume contours on (a), (b), (d), (e) and (f) are at $20 \text{ mm}^3 \text{ m}^{-3}$ intervals up to 100, $50 \text{ mm}^3 \text{ m}^{-3}$ intervals up to 600 and $100 \text{ mm}^3 \text{ m}^{-3}$ intervals above that. H marks “holes” (areas of lower concentration) on (d) which match areas of high concentration on (e) and (f).

mapped at 160 m in Fig. 9b. Part of the biovolume exhibits diel migration (Fig. 10), though this is only clearly apparent in the FSS (Fig. 6d), while the spatial patterns remain strongly constrained by the locations of the fronts (Fig. 9b).

Diel migration can be inferred on Fig. 6 by the very low biovolumes (usually less than the $40 \text{ mm}^3 \text{ m}^{-3}$ contour) within the concave isolines (solid white lines) that mark periods of daylight. At night, biovolume increases at depths around 50 m, weakly in Run 3 (Fig. 6a), increasing to clearly defined swarms by the end of the FSS (Fig. 6d, day 370.0). The extent of diel migration is quantified in Fig. 10. Compare the day- and night-time profiles for the CSS (Fig. 10a) for this size class. At all depths below 100 m, night-time biovolume densities are smaller than day-time ones. Above that depth, the opposite is true. If we assume that all the biovolume change below

100 m is the result of vertical migration, we calculate that $6500 \text{ mm}^3 \text{ m}^{-2}$ have migrated into the surface layer. However, the corresponding night-time increase in vertically integrated biovolume above 100 m is only $3200 \text{ mm}^3 \text{ m}^{-2}$, about half of $6500 \text{ mm}^3 \text{ m}^{-2}$, and the difference has to be ascribed to spatial variability. From examination of Fig. 10a it is clear that much larger differences than this were spatial for the 0.5–1 mm size class. So there may be no diel migration at all but we can say that at most 11% of the biovolume migrates.

The FSS presents a more definitive picture, as Fig. 6c shows a clear diurnal pattern in the surface layer. The day and night profiles (Fig. 10b) again show a reduction in night-time biovolume density at all depths below 70 m, and this time there is a clear night-time peak between 20–50 m. The night-time loss of biovolume below 70 m is $4000 \text{ mm}^3 \text{ m}^{-2}$, while the vertically integrated

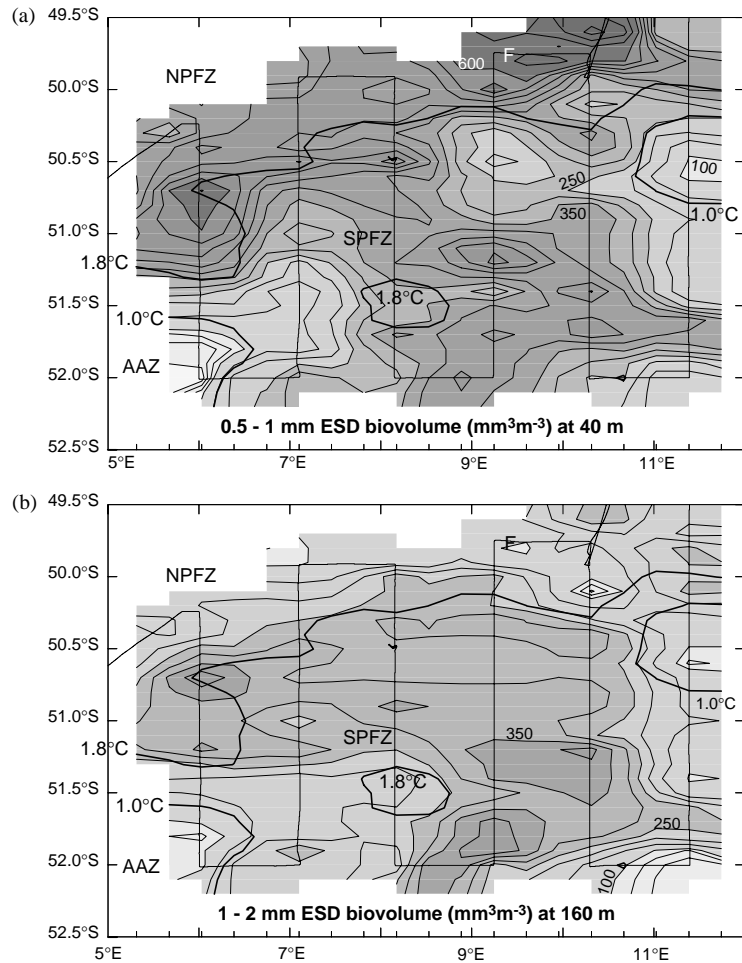


Fig. 9. Coarse Scale Survey area maps of (a) 0.5–1 mm ESD at 40–50 m, (b) 1–2 mm ESD at 150–170 m. Biovolume contours are the same as for Fig. 8.

day- and night-time biovolumes (respectively 41,200 and 41,600 mm³m⁻²) differ by only 400 mm³m⁻². While it is perhaps fortuitous that the integrated values are so close, we can again conclude that about 10% of the biovolume in this size class migrates from depths between 70 m and at least 360 m on a daily basis to feed in the surface layer.

5.4. 2–4 mm ESD

The largest copepod species in this size class is *Rhincalanus gigas*, for which adult females were measured at around 3.3–3.7 mm ESD and adult

males at 2.6–3.1 mm ESD. Stage V of *R. gigas* and adults of *Calanoides acutus* and *Calanus propinquus* also fall into the lower end of this class. At stations in the FSS, typically 5–20 ind m⁻³ of *R. gigas* were found for adults and stages C IV and V. At an ESD of 3 mm, 10 ind m⁻³ would equate to a biovolume of 130 mm³m⁻³, sufficient to explain the biovolume densities in Fig. 7.

Fig. 7 is rather patchy because the average abundance with 20 m by 1-h bins is only 4 individuals per bin. Despite this, diel migration is clear for all runs, with biovolume density increasing each night in a broad peak (labelled N in Fig. 7) spanning the depth range 40–100 m. This

Table 3
Major species and stages of copepods in each ESD size class

| ESD (μm) | Copepod species | Stage |
|--------------------------|------------------------------|---------------|
| 250–500 | <i>Oithona species</i> | Adult females |
| | <i>Microcalanus pygmaeus</i> | Adult females |
| 500–1000 | <i>Ctenocalanus</i> | Adult females |
| | <i>Clausocalanus</i> | Adult females |
| 1000–2000 | <i>Metridia lucens</i> | Adult females |
| | <i>Metridia gerlachei</i> | Adult females |
| | <i>Pleuromamma robusta</i> | Adult females |
| | <i>Calanoides acutus</i> | C IV |
| | <i>Calanoides acutus</i> | C V |
| | <i>Calanus simillimus</i> | C IV |
| | <i>Calanus simillimus</i> | Adult females |
| | <i>Calanus propinquus</i> | C IV |
| | <i>Rhincalanus gigas</i> | C III |
| <i>Rhincalanus gigas</i> | C IV | |
| 2000–4000 | <i>Rhincalanus gigas</i> | C V |
| | <i>Rhincalanus gigas</i> | Adult females |
| | <i>Rhincalanus gigas</i> | Adult males |
| | <i>Calanoides acutus</i> | adult females |
| | <i>Calanus propinquus</i> | Adult females |

peak is also clear in the averaged night-time profiles in Fig. 10. Below 100 m the averaged profiles all increase downwards to a maximum below 300 m. Densities in the upper 100 m are very low by day (excepting the top 10 m, which we shall discuss shortly), but increase considerably by night. The same calculations as for the 1–2-mm size class for the CSS show $2600 \text{ mm}^3 \text{ m}^{-2}$ being lost from below 120 m by night and $3400 \text{ mm}^3 \text{ m}^{-2}$ gained above 120 m (out of a total of around $18000 \text{ mm}^3 \text{ m}^{-2}$). The corresponding numbers for the FSS are $2500 \text{ mm}^3 \text{ m}^{-2}$ lost below and $3100 \text{ mm}^3 \text{ m}^{-2}$ gained above 120 m by night (out of a total of over $14,000 \text{ mm}^3 \text{ m}^{-2}$). Thus the biovolume migrating is several times greater than the discrepancy between day- and night-time integrated values and 15–18% of the standing stock.

Unexpected behaviour is apparent in the top-most bin (average of 0–10 m) in Fig. 7, and confirmed by the 2 m vertical resolution of Fig. 10. Biovolume densities increase rapidly upwards from 10 m to the surface, with surface values

about twice as large by day than by night. Note how the nocturnal concentrations (marked N in Fig. 7) are frequently linked to the surface at dawn and dusk. The inference is that animals are rising to the surface by day and descending to feed at night. Such behaviour has been reported from subtropical latitudes (Bollens et al., 1993; Mauchline, 1998; Ohman et al., 1983) but to the authors' knowledge not from high latitudes. However *R. gigas* is a likely candidate for such a feeding and predator avoidance strategy, as it is transparent and frequently remains motionless for long periods. By rising to the surface by day it would avoid predation by krill (*Thysanoessa* sp), whose presence is inferred from ADCP backscatter (Vélez et al., 2002) and which cannot themselves rise to the surface as they would be easily visible to avian predators (because of their activity and colouration).

5.5. Zonation

We have shown that diel migration only applies to a small fraction of the zooplankton population sampled by the OPC, with no diel behaviour apparent for ESDs $< 1 \text{ mm}$, and only 10–20% of the biovolume exhibiting diel migration for larger size classes. Thus little bias will be introduced by ignoring day-night variations and averaging the size classes spatially within various physical regimes. To create the profiles in Fig. 11, therefore, we have averaged the data for each size class at each pressure level of the $20 \text{ m} \times 1 \text{ h}$ gridded data set (Figs. 4–7) within each of the three zones described earlier (AAZ, SPFZ and NPFZ) and for each of Runs 3, 6 and 8. From Table 1 we see that the runs allow us to infer some temporal progression, as Run 6 was about two weeks after Run 3 and Run 8 was about a week later. Note that only one set of profiles has been created for Run 3 in the PFZ. This is because the PFZ was crossed in only 14 h and the temperature minimum was close to 1.8°C across the whole of the zone (from the start of Run 3 to 51.7°S). Vertically integrating each profile and converting to zooplankton carbon results in Table 4. The calibration will be described in the next section, but here it is the relative magnitudes in Table 4 that we shall discuss.

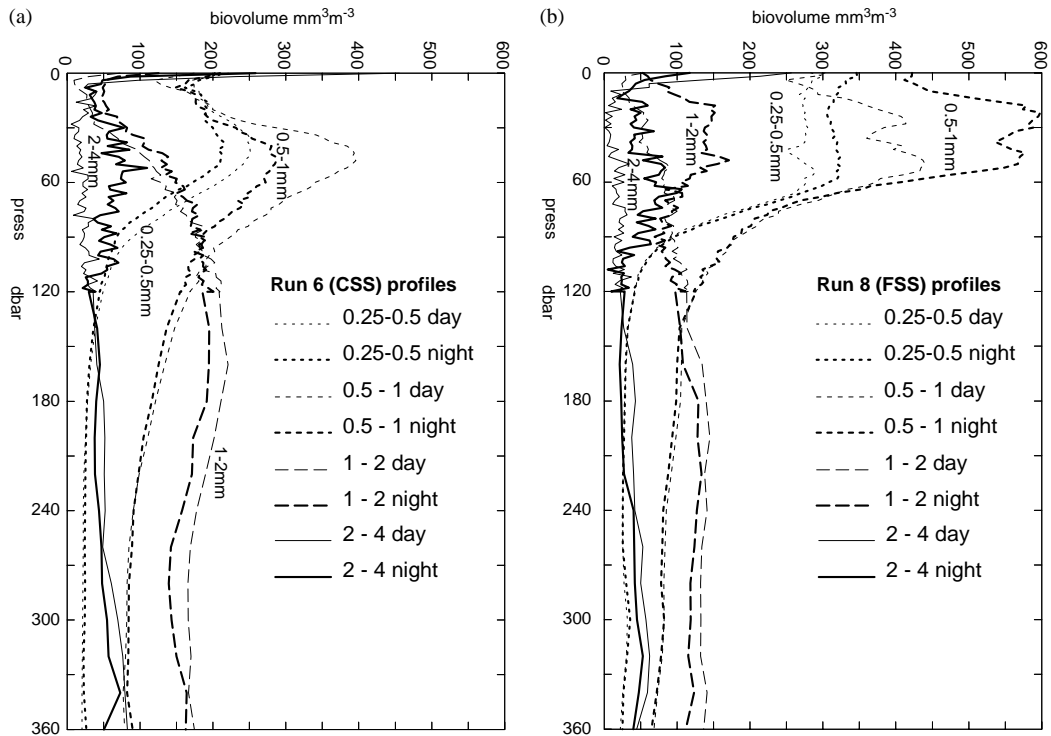


Fig. 10. Profiles of zooplankton biovolume for (a) the Coarse Scale Survey and (b) the Fine Scale Survey. For each survey there are four day-time profiles and four night-time profiles (bold lines), for the ESD size classes 0.25–0.5 mm (dots), 0.5–1 mm (short dashes), 1–2 mm (long dashes) and 2–4 mm (solid lines). Night-time profiles are obtained from all data between 1930 and 0330 GMT (approximately evenly spread about local midnight), and day-time the remainder. Below 120 m the profiles were obtained from the 1 h by 20 m gridded data used in Figs. 4–7. Above 120 m, greater vertical resolution was obtained by regridding the data into 2 m bins in the vertical.

Note first how the biovolume gradually moves upward through the water column with time for the two smaller size classes. For 0.25–0.5 mm ESD the maximum biovolume concentration lies between 60–80 m for Run 3, shallows to 40–60 m for Run 6, and is evenly spread from 0–60 m for Run 8. The depth below which the concentration remains at a low, baseline value of about $30 \text{ mm}^3 \text{ m}^{-3}$ also shallows, from about 180 m (Run 3) through 140 m (Run 6) to 100 m (Run 8). This progression is suggestive of seasonal upward migration (a few tens of metres in three weeks) of cyclopoid copepods such as *Oithona* spp. in the smallest size class.

Upward migration of the 0.5–1-mm ESD class has already been noted and is quantified by Fig. 11. During Run 3, the peak concentration is

at about 120 m in the AAZ, deeper than for the smaller size class. In the PFZ, however, a shallower peak is also apparent at 60 m (compare Fig. 5a). By Run 8 the peak concentration has risen to 40–60 m but tends to remain subsurface, in contrast to the smaller size class. Copepods in this size class (e.g., *M. lucens*) have thus migrated upwards by about 60 m in 3 weeks.

Much larger than the temporal changes are the spatial distributional differences between the three frontal zones. Integrated concentrations for 0.25–0.5 mm ESD nearly double from the AAZ ($0.42\text{--}0.50 \text{ g C m}^{-2}$, Table 4) to the SPFZ ($0.70\text{--}0.97 \text{ g C m}^{-2}$), with a further 20–40% increase from the SPFZ to the NPFZ. For 0.5–1 mm ESD, concentrations increase by 30–80% from the AAZ to the SPFZ and by a further 25%

Table 4
Zooplankton carbon (g C m^{-2}) by size, area and time

| | Run 3 | Run 6 | Run 8 |
|---------------------|-------|-------|-------|
| 0.25–0.5 mm ESD | | | |
| NPFZ | | 1.00 | 1.18 |
| SPFZ | 0.87 | 0.70 | 0.97 |
| AAZ | 0.47 | 0.42 | 0.50 |
| 0.5–1.0 mm ESD | | | |
| NPFZ | | 1.99 | 2.24 |
| SPFZ | 1.55 | 1.58 | 1.74 |
| AAZ | 1.16 | 1.19 | 0.96 |
| 1–2 mm ESD | | | |
| NPFZ | | 1.68 | 1.28 |
| SPFZ | 1.34 | 2.13 | 1.40 |
| AAZ | 1.04 | 1.17 | 0.68 |
| 2–4 mm ESD | | | |
| NPFZ | | 0.57 | 0.44 |
| SPFZ | 0.43 | 0.67 | 0.45 |
| AAZ | 0.28 | 0.32 | 0.38 |
| Total 0.25–4 mm ESD | | | |
| NPFZ | | 5.24 | 5.14 |
| SPFZ | 4.19 | 5.08 | 4.56 |
| AAZ | 2.95 | 3.10 | 2.52 |

from the SPFZ to the NPFZ. No doubt these changes relate to food availability in the form of phytoplankton. We shall consider these relationships in the final section.

Rather different behaviour is apparent for the larger size classes 1–2 and 2–4 mm ESD. Profiles of the latter (compare Fig. 10) have been omitted from Fig. 11 for clarity but vertically integrated values are included in Table 4. Zooplankton in the 1–2 mm ESD size class have peak concentrations well beneath the surface layer for all Runs and zones. Nevertheless, some upward shift is apparent in the depth below which concentrations increase to the subsurface peak. For Run 3, concentrations are uniformly low above 90 m. By Run 6 the concentrations start to increase downwards from as shallow as 20 m.

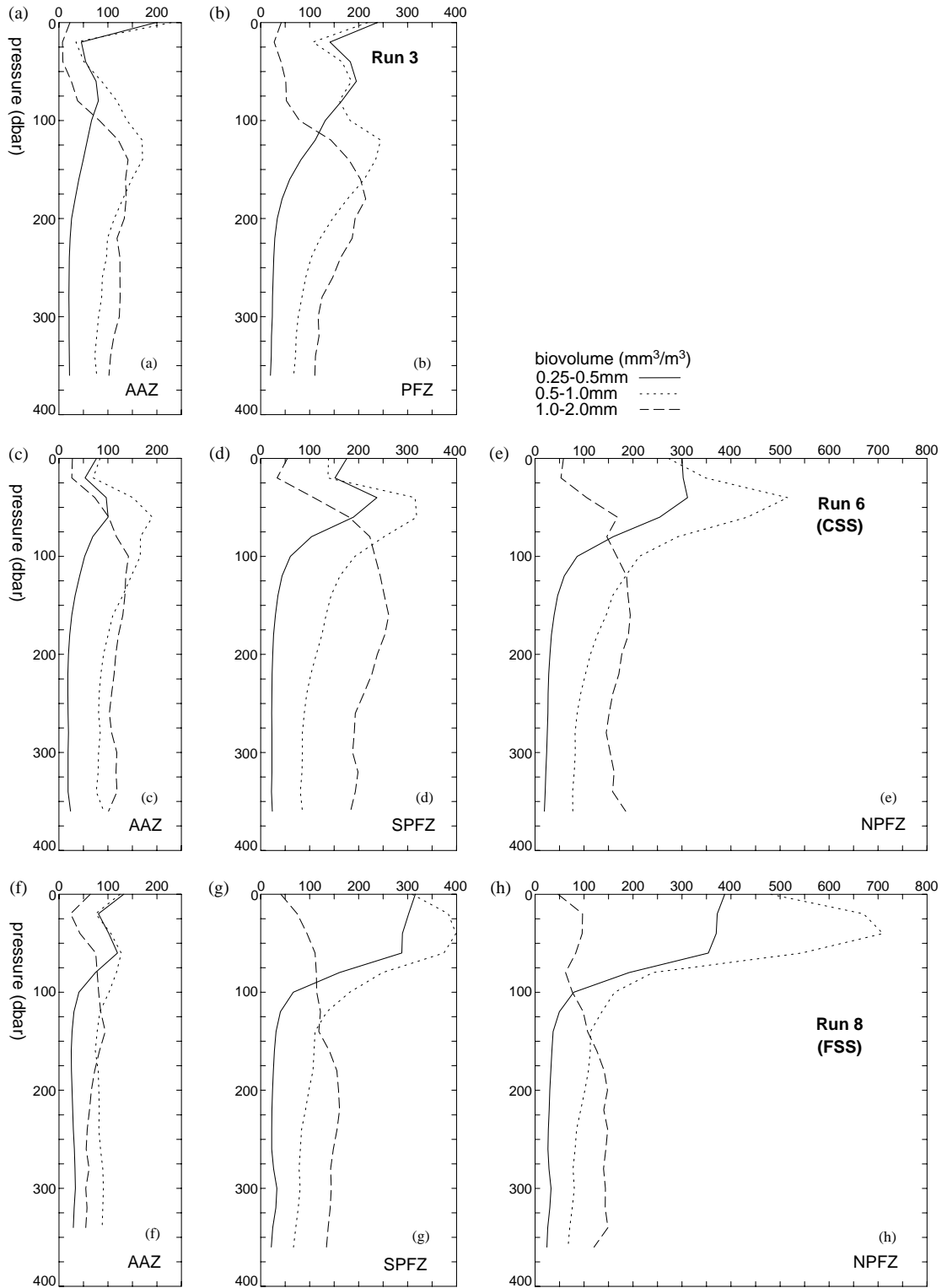
It is worth noting that the AAZ profiles for Runs 3 and 6 are closely matched in space (Fig. 1) because Run 6.1 (in which most of the Run 6 AAZ data were found, Fig. 1b) returned north along exactly the same track as Run 3 (running south-

ward) about 2 weeks later (Table 1). The two smaller size classes show no significant changes in biovolume from Run 3 (AAZ) to Run 6 (AAZ) but the profiles shift upwards. The 1–2 mm ESD size class shows a 12% increase (Table 4, 1.17/1.04), but the upward shift in the profile dominates, indicating that all zooplankton with ESDs < 2 mm are migrating upwards. As always, while we believe that this is the most likely explanation, we cannot rule out the possibility that the changes are purely advective, with new water masses with different populations having been advected into the region between the two runs.

Another major difference between the two smaller and two larger size classes is that the vertically integrated concentrations in the PFZ are *smaller* for Run 8 than for Run 6 and are *larger* in the SPFZ than in the NPFZ. Examining Figs. 1 and 9, it is likely that the differences are related to the different physical regimes. In Run 6 the SPFZ covered an extensive area between the surface expression of the APF (the 1°C temperature minimum) and the 1.8°C temperature minimum. Also, the 1°C contour followed a contorted path with, we infer, a large meander to the south near 6°E returning to the north somewhere east of 11°E. While there are both cyclonic and anti-cyclonic eddies apparent within the SPFZ, the dominant advective through-flows occur (Strass et al., 2002) at the southern and northern boundaries of the zone. Thus we speculate that larger copepods thrive in areas of low mean advection (eddies) adjacent to the major fronts that provide their main food source, the phytoplankton and smaller zooplankton that are advected through the area along those fronts. How they reach those areas will be considered later.

6. Calibration to carbon densities

In order to examine the ability of the OPC to count zooplankton and to convert biovolumes to carbon units, comparisons have to be made with net data, which, by their nature, have to be collected at a different time and place from the underway SeaSoar-mounted OPC. Now that the zooplankton distributions have been described



with respect to the physical environment, we are in a position to use that knowledge to create as many comparisons as possible. These comparisons are listed in Table 5 and described here.

While the Multinet collected data in five vertical bins down to 500 m, we found it impossible to obtain useful comparisons while retaining vertical resolution. In the top three multinet bins (0–25, 25–50 and 50–100 m) there were two problems. One was that the transition points between bins (25, 50 and 100 m) tended to coincide with depths at which zooplankton concentrations in the dominant size classes (0.5–1 mm and 1–2 mm ESD) were large (Fig. 11). The second was that it proved impossible to separate zooplankton from phytoplankton by filtering because of the large quantities of chain-forming silicious diatoms at many stations, particularly in the NPFZ. Concentrating on the deeper bins (100–300 and 300–500 m) was equally problematic because much biovolume for OPC ESDs <1 mm was concentrated in the upper 100 m (Fig. 11). A further problem was that diel migration of the larger size classes (Fig. 10) would bias the net data from individual stations. We have therefore restricted intercomparisons to vertical integrals of zooplankton concentration.

Half of each net sample was divided into different size fractions (100–200, 200–500, 500–1000, 1000–2000 and over 2000 μm) and each was filtered onto pre-weighed, pre-combusted (24 h at 550°C) filters for dry weight (DW) measurements. After being dried for 24 h at 50°C, the samples on the filters were stored at –20°C. Back in the home institute, filters were again dried for 24 h at 50°C and then weighed again. However, this dry weight measurement was not possible for many stations from which the near-surface filters were clogged with phytoplankton. Thus, there were only eight stations (6, 7, 9, 15, 16, 17, 18, and 22, Table 5 and Fig. 1) for which complete vertical profiles of dry

weights exist for all size classes, and indeed for two of these (16 and 22) we have extrapolated the 25–50 m values to the top 25 m. From these, we have created the five comparisons in Table 5:

- (1) Station 6 (Fig. 1a) is compared with the PFZ profile for Run 3 (Fig. 11b).
- (2) Station 7 (Fig. 1a) is compared with the last 8 h of Run 3 (Run 3 south, Table 5).
- (3) Station 9 (Fig. 1b) is compared with Run 6 profiles in the AAZ (Fig. 11c).
- (4) Station 15 (Fig. 1b) was clearly in the AAZ near the FSS, and so is compared with the Run 8 AAZ profile (Fig. 11f).
- (5) The remaining stations 16, 17, 18 (Fig. 1b) and 22 (Fig. 1c) all lie in the SPFZ area covered by Run 6 and close to the SPFZ area of Run 8. These four stations are separately tabulated in Table 5 along with the SPFZ profiles for Runs 6 and 8 (Figs 11d and g), and the average of the four stations is compared with the average of the two Runs.

We need to match the zooplankton size classes obtained from the filtered data with those from the OPC. If we assume that the filters trap copepods whose lengths match the filter mesh, and that copepod length is approximately twice the ESD, as discussed earlier, then the filter sizes and ESDs match as aligned in Table 5. The two smallest filters equate to copepod lengths that the OPC cannot resolve. The three largest OPC size classes (1–2, 2–4 and 4–8 mm ESD), on the other hand, are all covered by the largest filter, for lengths >2 mm. Confidence in this match is provided by examining the depth dependence (not shown) of the net dry weight concentrations (mg m^{-3}) of all the filter size classes. The only filter for which the dry weight concentrations do not decrease markedly below 100 m is the largest, for lengths >2 mm. Thus 2 mm length approximately matches

Fig. 11. Profiles of zooplankton biovolume for the three ESD size classes 0.25–0.5 mm (solid line), 0.5–1 mm (short dashes), and 1–2 mm (long dashes) are shown for Runs 3, 6 and 8 and for the Antarctic Zone (AAZ), Southern Polar Frontal Zone (SPFZ) and Northern Polar Frontal Zone (NPFZ). Thus time increases from top to bottom of the figure, and latitude runs roughly from south (AAZ) to north (NPFZ) across the figure from left to right. The fourth size class, 2–4 mm ESD, is not plotted, but is incorporated in Table 4, comprising the integrated carbon values from each profile.

Table 5
Comparisons of carbon from net and OPC

| Filtered length range (μm) ESD range (mm) | 100–200 | 200–500 0.25–0.5 | 500–1000 0.5–1 | 1000–2000 1–2 | Over 2000 2–4 | 4–8 | | Over 500 0.25–8 | Net/OPC Ratio |
|---|---------|---------------------|-------------------|------------------|------------------|------|------|--------------------|------------------|
| Run or station | | | | | | | | | |
| Station 6 | 1.75 | 1.14 | 1.47 | 0.87 | 0.65 | | | 2.99 | |
| Run 3 SPFZ | | | 1.45 | 2.59 | 2.24 | 0.71 | 0.24 | 7.23 | 0.41 |
| Station 7 | 0.50 | 0.51 | 0.47 | 0.49 | 0.81 | | | 1.77 | |
| Run 3 south | | | 0.26 | 0.51 | 0.56 | 0.49 | 1.20 | 3.03 | 0.59 |
| Station 9 | 0.57 | 0.89 | 2.25 | 1.66 | 1.46 | | | 5.37 | |
| Run 6 AAZ | | | 0.70 | 1.99 | 1.95 | 0.53 | 0.33 | 5.49 | 0.98 |
| Station 15 | 0.46 | 0.75 | 0.59 | 0.64 | 1.30 | | | 2.53 | |
| Run 8 AAZ | | | 0.84 | 1.60 | 1.14 | 0.64 | 0.15 | 4.36 | 0.58 |
| S16/17/18/22 | 0.50 | 0.58 | 1.39 | 0.90 | 1.01 | | | 4.38 | |
| Run 6/8 SPFZ | | | 1.39 | 2.76 | 2.94 | 0.93 | 0.29 | 8.31 | 0.40 |
| Station 16 | 0.48 | 0.55 | 1.84 | 1.60 | 0.83 | | | 4.27 | |
| Station 17 | 0.60 | 0.71 | 0.97 | 0.38 | 0.93 | | | 2.28 | |
| Station 18 | 0.56 | 0.68 | 1.61 | 0.72 | 1.14 | | | 3.47 | |
| Station 22 | 0.35 | 0.38 | 1.12 | 0.91 | 1.14 | | | 3.17 | |
| Run 6 SPFZ | | | 1.16 | 2.63 | 3.55 | 1.11 | 0.45 | 8.90 | |
| Run 8 SPFZ | | | 1.61 | 2.90 | 2.33 | 0.75 | 0.13 | 7.71 | |

Notes:

(1) Tabulated values are nominally carbon in units of gCm^{-3} .

(2) For net (station) data, carbon is taken to be 50% of dry weight.

(3) For OPC data, carbon is taken to be 50% of dry weight, dry weight is taken to be 10% of wet weight, and wet weight (g) is taken to be equivalent to biovolume (cm^3).

1 mm ESD, at which the changeover in OPC vertical structure occurs (Fig. 11).

Finally, we have to convert dry weight concentrations and OPC biovolume to carbon concentrations. It is fairly well established that the carbon content of Antarctic copepods is close to 50% of the dry weight (Mizdalski, 1988), so this factor has been used to give definitive carbon concentration values for the stations in Table 5. Several formulae are found in the literature to convert wet weights to carbon. Most are derived from net data (Wiebe, 1988; Wiebe et al., 1975) so are designed to take into account the volume of interstitial water trapped by capillary action between animals and their appendages in net samples. This leads to non-linear relationships between displacement volume, wet weights and dry weights (e.g., Rodriguez and Mullin, 1986; used by Huntley et al., 1995). These are inappropriate for OPC data, in which the shadow of each individual has been measured. We therefore have converted linearly from biovolume

concentration (or displacement volume) as presented in this paper into carbon concentration by the following simple assumptions:

- wet weight in grams is the same as displacement volume in cc, i.e. the zooplankton are neutrally buoyant, true within a few percent,
- dry weight is 10% of wet weight,
- carbon is 50% of dry weight.

Given the considerable differences caused by spatial patchiness (compare nets 16 and 17, for example), the comparisons in Table 5 between net and underway OPC data are encouragingly close. For the 15 bins for which there are both net and OPC values (5 stations each with 3 matching size classes), 8 have larger OPC values, 4 have larger net values, and in 3 the values are nearly equal. The tendency, though, is for OPC values to be on the large size. As there are numerous sources of error in matching size classes, we have chosen not to match individual bins, but have summed the

rows of Table 5 for lengths $> 500 \mu\text{m}$, ESDs $> 250 \mu\text{m}$, and presented their ratios (net/OPC) in the last column. There are two values of 0.4, two values of 0.6 and one value of 1.0. The last arises from anomalously high net carbon values at Station 9, the highest of all stations in the Table, yet Station 9 is in the generally low biomass AAZ. Arguments also can be advanced to suggest that the values of 0.4 are rather low. Our final choice is to use the mean (or median) of the 5 ratios, 0.6, as the scaling value for OPC data. This value is very close to that determined by Sprules et al. (1998), who scaled their spherical biovolumes by a factor $f^{-2} = 0.57$ for their best fit of $f = 1.33$ after careful field and laboratory calibrations. Although their data were for fresh-water species, their experimental setup was very similar to ours in that their OPC had a similar aperture and their count rates (up to $100 \text{ counts s}^{-1}$) were also similar. The count rate determines the probability of coincidence counts (which they discuss in detail) and hence the value of f .

In summary, five separate comparisons suggest that the OPC based estimates of zooplankton carbon need to be scaled by a factor somewhere between 0.4 and 1.0, and we have opted for a scaling of 0.6. Given the considerable difficulty in obtaining quantitative calibrations, we consider that calibration within a factor of two is very satisfactory, and the OPC is within this range even before applying the 0.6 scaling. Finally, whatever the scaling factor applied to OPC data, there is one important conclusion we may draw from Table 5, from the net-derived dry-weight calculations alone. The total biovolume (and species numbers) of copepods in the PFZ in the South Atlantic is at least a factor of two higher than reported previously (Fransz and Gonzalez, 1997). To consider the causes for this high concentration of copepods, we must next discuss their relationships with each other and with physics and phytoplankton.

7. Discussion—biophysical and biological interactions

We consider now relationships between zooplankton size classes, between zooplankton and

phytoplankton, and between all of these and the physical regimes. The primary figures to be used are the maps of the CSS and FSS in Figs. 8 and 9. We also introduce a map of phytoplankton carbon derived from near-surface chlorophyll (Fig. 12a). (For later comparison with zooplankton carbon, the chlorophyll has been mapped in carbon units by assuming that the near-surface (8 m deep) values extend through the top 70 m (confirmed by SeaSoar fluorescence, not shown) and that 1 mg m^{-3} of chlorophyll equates to 50 mg m^{-3} of carbon (e.g., Maranon et al. (2000) Thus 1 mg chl m^{-3} is contoured as 3.5 g C m^{-2}). Chlorophyll distributions from OPC attenuation measurements calibrated against towed and underway fluorimeters and from the extracted samples are discussed in detail elsewhere (Strass et al., 2002) Here, it is sufficient to map chlorophyll as determined from direct measurements every 3 h while underway and from the shallowest bottles from CTD casts. Thus Fig. 12a is the master chlorophyll calibration data set covering all data from before, during and after both the FSS and CSS. Chlorophyll values changed little with time, and overall provide enough spatial coverage to produce a representative map. The major features of Fig. 12a are the relatively high chlorophyll concentrations in bands where there is strong advection (compare Pollard et al., 1995) and the areas of weak concentration in the AAZ and indeed over much of the SPFZ.

7.1. Physical influences on zooplankton distributions

Fig. 8 compares the spatial distributions for three zooplankton size classes at the surface (0–5 m) and in the surface layer (20–30 m) for Run 8. It is clear that the two smaller size classes, 0.25–0.5 and 0.5–1 mm ESD, are predominantly advected by the circulation, as the currents (Naveira Garabato et al., 2001; Strass et al., 2002) run clockwise (cyclonically) around the cold AAZ feature in the southeast corner of the FSS (bounded by the 1°C isotherm marked on Fig. 8) and also run from west to east across the FSS in the NPFZ (north of the 1.8°C isotherm). More interesting is that in the surface layer the 1–2 mm

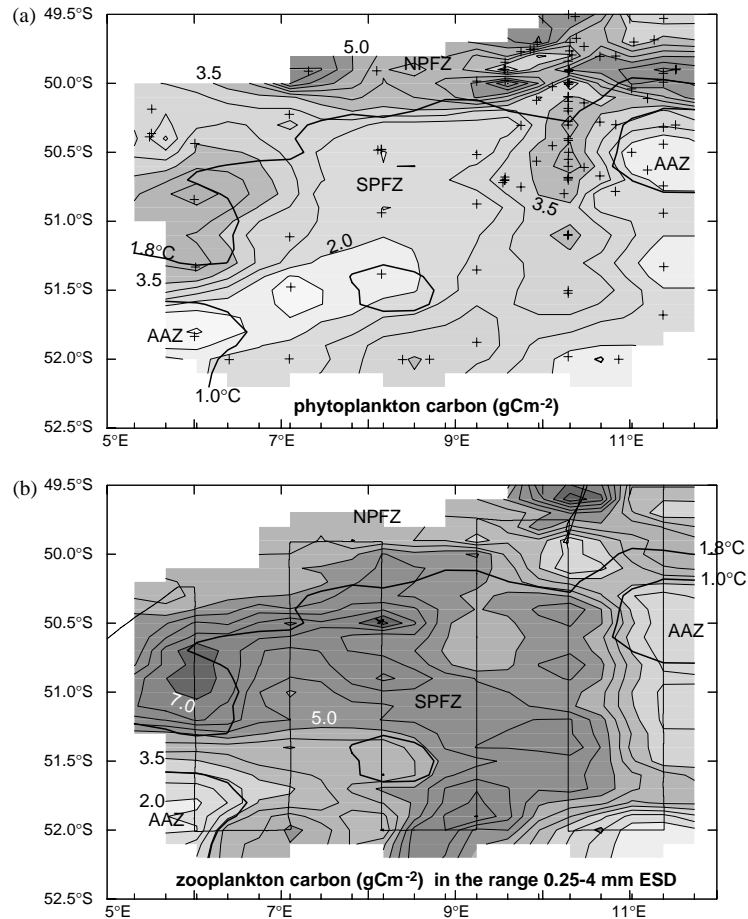


Fig. 12. Maps of (a) phytoplankton carbon and (b) zooplankton carbon in the Coarse Scale Survey area. Phytoplankton carbon is derived from chlorophyll samples drawn from the pumped clean sea water supply (intake at 8 m depth) every 3 h while underway, and these have been supplemented by data from the shallowest bottles (usually 10 m) on CTD casts. Sample points are marked by plus (+) symbols. Obviously, areas with sparse data points must be interpreted with caution. The carbon units of gCm^{-2} have been derived from chlorophyll by a linear scaling of 3.5 (see text). Thus 3.5 gCm^{-2} equates to $1.0 \mu\text{g l}^{-1}$ chlorophyll. Zooplankton carbon is the vertical integral from 0–360 m of biovolume in the size classes spanning ESDs of 0.25–4 mm, scaled as discussed in the text. The track plot along which data were collected is shown on (b). Bold lines are the 1.0°C and 1.8°C temperature minimum isotherms.

ESD class (Fig. 8f) (comprising *M. lucens*, *P. robusta*, larger stages of *R. gigas*, and others—Table 3) does not track the surface currents, but is dominated by diel migration.

Most of the biovolume of the 1–2 mm ESD size class resides much deeper in the water column (Fig. 6), and a map for the CSS at 160 m, the depth at which biovolume densities are largest (Fig. 9b), shows strong correlation with the physical structure. Again, the 1.0°C and 1.8°C

isotherms marking the fronts are useful boundaries, and it is seen that, over the whole of the CSS (Fig. 9b), biovolume in this size class is primarily concentrated between these two isotherms, which we have termed the SPFZ. Biovolume clearly drops away in the AAZ (south of the 1.0°C isotherm), but somewhat surprisingly, it tends to decrease in the NPFZ (north of the 1.8°C) also. The question then arises, how do these larger copepods find their food sources,

phytoplankton and perhaps smaller zooplankton? The likely answer to this question and an explanation for the spatial distributions lies in the ageostrophic circulation associated with the fronts.

As described by Strass et al. (2002) and Naveira Garabato et al. (2001), there is a pressure ridge running from north to south down approximately the centre of the CSS, as we can infer from the somewhat warmer temperatures (Fig. 1b) along 8°E compared to 11°E and the southern end of 6°E. The geostrophic circulation resulting from this pressure ridge is the northward flow along about 10°E. The associated ageostrophic circulation will consist of eastward flow across 10°E in the surface layer balanced by westward flow beneath the surface layer and consequently upwelling in the centre of the CSS west of 10°E and downwelling east of 10°E. The ageostrophic horizontal velocities are only a few cm s^{-1} (Naveira Garabato et al., 2001; Strass et al., 2002), but over a week or more the eastward surface flow will tend to create the band of relatively high phytoplankton densities along 10°E (Fig. 12a) as the phytoplankton grow and move eastwards in the surface layer.

Within the zooplankton, the smaller animals (0.25 to 1 mm ESD) confined to the surface layer will be advected much as the phytoplankton are. Copepods larger than 1 mm ESD, on the other hand, spend most of their time beneath the surface layer, so will be gradually advected westward across 10°E into the centre of the CSS (Fig. 9b). That small fraction (10%) of the larger copepods that displays diel migration will alternate between eastward and westward transport, so will tend to remain closer to the surface layer food source, as shown by the tendency to larger concentrations along the same bands as the phytoplankton maxima (compare Fig. 9b with Fig. 12a). This retentive circulation is reminiscent of behaviour that has been observed in coastal upwelling systems Painting et al. (1993) where zooplankton (e.g., *Ctenocalanus vanus*, *Calanoides carinatus*) are believed to make use of the deep on-shore and shallow off-shore flows to maintain their distribution within a high food availability region.

7.2. Biological influences on zooplankton distribution

Let us look now at the smallest size class, 0.25–0.5 mm ESD. These are present in large concentrations (over $10,000 \text{ ind m}^{-3}$) in the surface layer. The dominant copepod in this class, *Oithona* spp., is omnivorous, and is probably responsible for the removal of faecal pellets from larger zooplankton, which were notable by their absence in the net samples which were microscopically examined. The much smaller faecal material from *Oithona* would sink more slowly, consistent with the low export production that was observed (van der Loeff et al., 2002). The distribution of this size class in the surface layer closely follows the frontal features (Figs. 8a and d) and matches the chlorophyll distribution (Fig. 12a). It has also been noted that the surface distribution of the 0.25–0.5 mm ESD size class in the FSS (Fig. 8a) closely matches that of prions (van Franeker et al., 2002), indicating that the small copepods are a major food source for those seabirds.

Subtle but possibly significant differences are apparent between the 0–5 m and 20–30 m distributions (Figs. 8a and d), especially when compared with those for the next larger size class (Figs. 8b and e). Although the spatially averaged profiles show no differences between 0–5 m and 20–30 m (Figs. 11g and h) for the 0.25–0.5 mm class, there are “holes” (marked H) apparent in Fig. 8d at several positions where concentrations of the larger size classes (Figs. 8e and f) are maximum. There are two possible explanations. One is that there is vertical partitioning between the different size classes, with a fraction of the smallest size class moving up to the surface as the larger size classes migrate into the 40–50 m depths each night. This seems unlikely given our earlier discussion on the lack of diel migration for the smallest size class. Also, greater concentrations at the surface than at 20–30 m are apparent in the southeast corner of the FSS (the AAZ area in Figs. 8a and d) during both day and night-time periods (Fig. 8c). We therefore favour an alternative explanation, that there is some carnivorous predation of the smallest size class by the larger ones in these two areas. Copepods in the larger size classes such as

C. simillimus and *M. lucens* are known to be omnivorous and are probably large enough to capture the smaller copepods and copepodites.

7.3. Carbon concentrations

It is particularly interesting to compare estimates of phytoplankton and zooplankton carbon (Fig. 12). We have estimated the former as described earlier. Zooplankton carbon has been estimated by scaling biovolume by 0.6 as determined in the section on calibration, integrating from 360 m to the surface, and summing over the 4 ESD size ranges from 0.25–2 mm. Maps of the individual size classes (not shown) are spatially similar to Fig. 9a for the two smaller size classes and to Fig. 9b for the two larger classes. The largest carbon densities are similar for both phyto- and zooplankton, reaching around 6 g C m^{-2} along 50°S for phytoplankton in the NPFZ along the northern boundary and over 7 g C m^{-2} for zooplankton in several places. Over the CSS survey area as a whole, however, zooplankton carbon densities (Fig. 12b) are clearly greater than phytoplankton carbon densities (Fig. 12a). Let us examine the spatial distributions in more detail.

Consider first the AAZ. Both phytoplankton and zooplankton distributions exhibit low densities in the AAZ, seen in the far southwest corner of the CSS survey area and around 50.5°S along the eastern boundary. Yet silicate and nitrate were both plentiful in the AAZ (Hartmann et al., 1997), with near-surface (8 m depth) values of silicate over $20 \mu\text{M}$ and nitrate values over $24 \mu\text{M}$. This is the classic high nutrient, low chlorophyll scenario, so we assume that the low zooplankton concentrations are simply a consequence of the lack of phytoplankton food availability.

Consider next the two frontal zones bounding the SPFZ, the one running along the 1.8°C temperature minimum isotherm, the other entering the CSS on the south side at 9°E and running north along about 10°E . Along both frontal zones there is a tendency for both phytoplankton and zooplankton carbon concentrations to be enhanced. But the ratio of zooplankton to phytoplankton carbon varies considerably along the two fronts. West of 8°E or 9°E along the 1.8°C

isotherm zooplankton carbon is greater than phytoplankton carbon. The same is true along 10°E south of about 50.5°S , indicating in both cases that zooplankton grazing is well advanced in the sense that larger zooplankton have developed (Fig. 9b), which are capable of grazing at least some components of the siliceous diatom population that forms the bulk of the standing stock of phytoplankton carbon, and have reduced that standing stock. The situation is reminiscent of that reported by Read et al. (2002) in an eddy much further north. Clearly, in a local area one's intuition that biomass should decrease with increasing organism size needs refinement. Where it is possible for zooplankton to multiply in a confined area, their biomass can exceed that of phytoplankton once the latter are grazed down, resulting in the classic inverted trophic pyramid. Along the frontal zone north of 50.2°S (Fig. 12a) on the other hand, phytoplankton carbon is at its maximum, and in places exceeds zooplankton carbon. The contribution of larger zooplankton is smaller in this region (marked F in Fig. 9) than along the fronts further south and west (Fig. 9b), so the implication is that in this NPFZ region the larger zooplankton are not reducing phytoplankton standing stocks as they are along the fronts further south and west. Thus there is top-down control of the phytoplankton standing stock.

The results above suggest that zooplankton control of the phytoplankton standing stock is less advanced in the NPFZ than further south. Interestingly, this is not what might be expected from primary productivity calculations (Tremblay et al., 2002). In the NPFZ silicate concentrations are close to limiting for diatom growth, as low as $2 \mu\text{M}$ at the very northern limit of the CSS on legs 6.6 and 6.7 (Hartmann et al., 1997), and lower growth rates of phytoplankton were found there than further south (Tremblay et al., 2002). Thus, despite silica limitation of phytoplankton growth rates in the NPFZ, phytoplankton standing stock is higher because there is less zooplankton grazing. The SPFZ is therefore the more active region for both phytoplankton and zooplankton, with higher growth rates of phytoplankton (Tremblay et al., 2002) more grazing control by zooplankton and larger zooplankton standing stocks (Fig. 12b).

8. Summary and conclusions

Using 15 days of data comprising 22 million counts sampled underway along a 6000 km track with a towed OPC, we have examined the distribution of zooplankton in the vicinity of the Antarctic Polar Front and south of it as functions of horizontal location, depth, zooplankton size and time. The distribution and behaviour of zooplankton split into two main categories, those with ESD less than or > 1 mm, where 1 mm ESD equates approximately to an animal length of 2000 μm . Zooplankton smaller than 1 mm ESD were primarily confined to the surface layer, i.e. shallower than about 80 m by January. Spatially, their biovolume was greatest in frontal regions where there was significant advection. Zooplankton larger than 1 mm ESD, on the other hand, remained primarily beneath the surface layer and were most abundant in a large area of the SPFZ which lay between the major fronts. A small fraction (10–20%) of the biovolume of these larger zooplankton exhibited diel migration, rising to depths of 20–50 m by night. Some of the largest zooplankton (2–4 mm ESD) exhibited reverse migration, ascending apparently to the surface by day. Over the period of the cruise (early December to early January) there was evidence of gradual upward (seasonal) migration of zooplankton both larger and smaller than 1 mm ESD.

The dominant control on zooplankton biomass was location relative to the APF, which we determined by categorizing the area surveyed into three frontal zones. South of the surface expression of the APF (determined by the location of the 1.0°C subsurface temperature minimum) we named the Antarctic Zone (AAZ), north of that we called the Polar Frontal Zone, split into Southern (SPFZ) and Northern (NPFZ) sectors by the location of the 1.8°C temperature minimum. In the AAZ, zooplankton carbon densities were relatively low, 2.5 to 3 gCm^{-2} (Table 4), controlled by low food (phytoplankton) availability in this high nutrient low chlorophyll region. In the SPFZ and NPFZ densities were higher, 4 to 5 gCm^{-2} . These densities were at least a factor of 2 higher than observed in a similar survey three years earlier (Fransz and Gonzalez, 1997) and

were of similar magnitude to phytoplankton carbon densities. Biomass of the larger zooplankton (over 1 mm ESD) was larger in the SPFZ than in the NPFZ. These zooplankton are capable of grazing the siliceous diatoms that form the bulk of the phytoplankton standing stock, so their top-down control of phytoplankton carbon is greatest in the SPFZ.

Acknowledgements

We thank the chief scientist Victor Smetacek for the conceptual and practical guidance of the cruise and the captain, officers and crew of *Polarstern* for their expertise in often difficult conditions at sea. Much help with the SeaSoar and OPC was provided by Pat Gwilliam and John Smithers. Mike Griffiths organised the computing with expert help from the RVS computer group. The lead author is grateful to several colleagues for guidance and suggestions, including Alex Mustard, Howard Roe, John Allen and Tom Anderson.

References

- Allen, J.T., Fischer, H., Griffiths, M.J., Pollard, R.T., Read, J.F., Strass, V.H., 1996. Acoustic Doppler Current Profiler data collected on *Polarstern* Cruise ANTARKTIS XIII/2 4 December 1995–24 January 1996. Southampton Oceanography Centre Internal report No. 2, 46pp.
- Bathmann, U.V., Scharek, R., C, K., Dubischar, C. D., Smetacek, V., 1997. Spring development of phytoplankton biomass and composition in major water masses of the Atlantic sector of the Southern Ocean. *Deep-Sea Research II* 44, 51–67.
- Belkin, I.M., Gordon, A.L., 1996. Southern Ocean fronts from the Greenwich Meridian to Tasmania. *Journal of Geophysical Research* 101, 3675–3696.
- Bollens, S.M., Osgood, K., Frost, B.W., Watts, S.D., 1993. Vertical distribution and susceptibilities to vertebrate predation of the marine copepods *Metridia lucens* and *Calanus pacificus*. *Limnology and Oceanography* 38, 1827–1837.
- Dubischar, C.D., Bathmann, U.V., 1997. Grazing impact of copepods and salps on phytoplankton in the Atlantic sector of the Southern Ocean. *Deep-Sea Research II* 44, 415–433.
- Dubischar, C., Bathmann, U., Menden-Deuer, S., Rynearson, T., 1997. Zooplankton dynamics. In: Bathmann, U., Lucas,

- M., Smetacek, V. (Eds.), Die Expedition ANTARKTIS XIII/1-2 des Forschungsschiffes "Polarstern" 1995/96. Alfred-Wegener-Institut für Polar- und Meeresforschung, Bremerhaven, pp. 102–106.
- Dubischar, C.D., Lopes, R.M., Bathmann, U.V., 2002. High summer abundances of small pelagic copepods at the Antarctic Polar Front - implications for ecosystem dynamics. *Deep-Sea Research II*, in press.
- Fransz, H.G., Gonzalez, S.R., 1997. Latitudinal metazoan plankton zones in the Antarctic Circumpolar Current along 6°W during austral spring 1992. *Deep-Sea Research II* 44, 395–414.
- Gallienne, C.P., Robins, D.B., Pilgrim, D.A., 1996. Measuring abundance and size distribution of zooplankton using the Optical Plankton Counter in underway mode. *Underwater Technology* 21, 15–21.
- Griffiths, M.J., Allen, J.T., Gwilliam, T.J.P., Naveira, A.G., Pollard, R.T., Read, J.F., 1996. SeaSoar operations and data collected on *Polarstern* Cruise ANTARKTIS XIII/2 4 Dec 1995–24 Jan 1996. Southampton Oceanography Centre Report No. 1, 86pp.
- Hartmann, C., Hollmann, B., Kattner, G., Richter, K.-U., Terbrüggen, A., 1997. Nutrients, dissolved and particulate matter. In: Bathmann, U., Lucas, M., Smetacek, V. (Eds.), Die Expedition ANTARKTIS XIII/1-2 des Forschungsschiffes "Polarstern" 1995/96. Alfred-Wegener-Institut für Polar- und Meeresforschung, Bremerhaven, pp. 44–52.
- Herman, A.W., 1988. Simultaneous measurement of zooplankton and light attenuation with a new optical plankton counter. *Continental Shelf Research* 8, 205–221.
- Herman, A.W., 1992. Design and calibration of a new optical plankton counter capable of sizing small zooplankton. *Deep-Sea Research* 39, 395–415.
- Herman, A.W., Sameoto, D.D., Shunniyan, C., Mitchell, M.R., Petrie, B., Cochrane, N., 1991. Sources of zooplankton on the Nova Scotia Shelf and their aggregations within deep-shelf basins. *Continental Shelf Research* 11, 214–236.
- Huntley, M.E., Zhou, M., Nordhausen, W., 1995. Mesoscale distribution of zooplankton in the California Current in late spring, observed by Optical Plankton Counter. *Journal of Marine Research* 53, 647–674.
- Maranon, E., Holligan, P.M., Valera, M., Mourino, B., Bale, A.J., 2000. Basin-scale variability of phytoplankton biomass, production and growth in the Atlantic Ocean. *Deep-Sea Research I* 47, 825–857.
- Mauchline, J., 1998. The biology of calanoid copepods. In: Blaxter, J.H.S., Southward, A.J., Tyler, P.A. (Eds.), *Advances in Marine Biology*, Vol. 33. Academic Press, San Diego CA.
- Metz, C., 1996. Lebensstrategien dominanter antarktischer Oithonidae (Cyclopoida, Copepoda) und Oncaeididae (Poecilostomatoida, Copepoda) im Bellingshausenmeer. *Reports on Polar Research* 207, 123pp.
- Mizdalski, E., 1988. Weight and length data of zooplankton in the Weddell Sea in austral spring 1986 (ANT V/3), xpp. *Reports on Polar Research* 55.
- Naveira Garabato, A., Allen, J.T., Leach, H., Strass, V.H., Pollard, R.T., 2001. Mesoscale subduction at the Antarctic Polar Front driven by baroclinic instability. *Journal of Physical Oceanography* 31, 2087–2107.
- Ohman, M.D., Frost, B.W., Cohen, E.B., 1983. Reverse diel vertical migration: an escape from invertebrate predators. *Science* 220, 1404–1407.
- Painting, S.J., Lucas, M.I., Peterson, W.T., Brown, P.C., Hutchings, L., Mitchell-Innes, B.A., 1993. Dynamics of bacterioplankton, phytoplankton and mesozooplankton communities during the development of an upwelling plume in the southern Benguela. *Marine Ecology Progress Series* 100, 35–53.
- Pollard, R.T., 1986. Frontal surveys with a towed profiling conductivity/temperature/depth measurement package (SeaSoar). *Nature* 323, 433–435.
- Pollard, R.T., Read, J.F., 2001. Circulation pathways and transports of the Southern Ocean in the vicinity of the Southwest Indian Ridge. *Journal of Geophysical Research* 106, 2881–2898.
- Pollard, R.T., Read, J.F., Allen, J.T., Griffiths, G., Morrison, A.I., 1995. On the physical structure of a front in the Bellingshausen Sea. *Deep-Sea Research II* 42, 955–982.
- Pollard, R.T., Griffiths, M.J., Gwilliam, T.J.P., Read, J.F., 1996. Optical Plankton Counter SeaSoar data collected on *Polarstern* Cruise ANTARKTIS XIII/2 4 Dec 1995–24 Jan 1996. Southampton Oceanography Centre Internal Report No. 3, 92pp.
- Pollard, R.T., Lucas, M.I., Read, J.F., 2002. Physical controls on biogeochemical zonation in the Southern Ocean. *Deep-Sea Research II* 49 (16), 3289–3305.
- Read, J.F., Pollard, R.T., Bathmann, U., 2002. Physical and biological patchiness of an upper ocean transect from South Africa to the ice edge at the Greenwich Meridian. *Deep-Sea Research*, this volume.
- Rodriguez, J., Mullin, M.M., 1986. Relation between biomass and body weight of plankton in a steady state oceanic ecosystem. *Limnology and Oceanography* 31, 361–370.
- Sheldon, R.W., Prakash, A., Sutcliffe, W.H.J., 1972. The size distribution of particles in the ocean. *Limnology and Oceanography* 17, 327–340.
- Sprules, W.G., Jin, E.H., Herman, A.W., Stockwell, J.D., 1998. Calibration of an optical plankton counter for use in fresh water. *Limnology and Oceanography* 43, 726–733.
- Strass, V.H., Naveira Garabato, A.C., Pollard, R.T., Fischer, H., Hense, I., Allen, J.T., Read, J.F., Leach, H., Smetacek, V., 2002. Mesoscale frontal dynamics: shaping the environment of primary production in the Antarctic Circumpolar Current. *Deep-Sea Research II*, this issue.
- Tremblay, J.E., Lucas, M.I., Kattner, G., Pollard, R.T., Bathmann, U.V., Strass, V., 2002. Significance of the Antarctic Polar Front for the production of biogenic carbon and silicon during early summer in the Southern Ocean. *Deep-Sea Research II*, this issue.

- van der Loeff, M.M.R., Buessler, K., Bathmann, U., Hense, I., Andrews, J., 2002. Steady summer production and a sudden spring bloom make a comparable contribution to carbon and opal export near the Antarctic Polar Front. Deep-Sea Research II, this issue.
- van Franeker, J.A., van den Brink, N.W., Bathmann, U.V., Pollard, R.T., De Baar, H.J.W., 2002. Responses of seabirds, in particular prions (*Pachyptila* sp.), to small scale processes in the Antarctic Polar Front. Deep-Sea Research II, this issue.
- Vélez, P., Allen, J.T., Strass, V.H., 2002. A new way to look at mesoscale zooplankton distributions: an application at the Antarctic Polar Front. Deep-Sea Research, this volume.
- Wiebe, P.H., 1988. Functional regression equations for zooplankton displacement volume, wet weight, dry weight and carbon: a correction. Fisheries Bulletin 86, 833–835.
- Wiebe, P.H., Boyd, S., Cox, J.L., 1975. Relationships between zooplankton displacement volume, wet weight, dry weight and carbon. Fisheries Bulletin 73, 777–786.